

University of Nevada, Reno

**Mitigating IPMC Back Relaxation Through Feedforward and Feedback
Control of Patterned Electrodes**

A thesis submitted in partial fulfillment of the
requirements for the degree of Master of Science in
Mechanical Engineering

by

Maxwell Jonathan Fleming

Dr. Kam K. Leang/Thesis Advisor

May 2012



University of Nevada, Reno
Statewide • Worldwide

THE GRADUATE SCHOOL

We recommend that the thesis
prepared under our supervision by

MAXWELL JONATHAN FLEMING

entitled

**Mitigating IPMC Back Relaxation Through Feedforward and Feedback
Control of Patterned Electrodes**

be accepted in partial fulfillment of the
requirements for the degree of

MASTER OF SCIENCE

Kam K. Leang, Ph. D., Advisor

Kwang J. Kim, Ph. D., Committee Member

Yantao Shen, Ph. D., Graduate School Representative

Marsha H. Read, Ph. D., Dean, Graduate School

May, 2012

Abstract

The goal of this thesis is to minimize the back relaxation behavior in ionic polymer-metal composite (IPMC) actuators. With low driving voltage ($<5V$) and the ability to be operated in aqueous environments, IPMCs have gained great attention in recent years for use in many applications including soft bio-inspired actuators and sensors. There are, however, drawbacks to IPMC actuators, including the “back relaxation” effect. Specifically, when subjected to an excessively slow dynamic input, the IPMC actuator will slowly relax back toward its original position. As this effect can cause excessive positioning error, it is important to compensate for the behavior to enhance applications in robotics and other bio-inspired systems. Methods do already exist to compensate for back relaxation, however they mostly involve undesirable fabrication processes or control methods with high voltage demands. By circumventing back relaxation using alternative means, any number of IPMC applications could be improved. For instance, IPMC-guided surgical tools could be controlled more precisely, gripping strength could be increased for an IPMC-powered hand prosthesis, and IPMC-based underwater autonomous systems could have enhanced maneuvering. The contribution of this work is the use of sectored IPMCs to mitigate back relaxation. This class of IPMC typically uses patterned electrodes to produce complex motion or even self-sensing capabilities. In this work, however, a new control technique is proposed, allowing the IPMC sectors to be actuated in opposite directions such that the back relaxation components counteract each other. A feedforward control method is designed around this concept and shown to effectively mitigate the back relaxation effect. Performance is further improved by integrating feedback control. Experimental results using a very slow reference and the integrated feedforward and feedback control method show a nearly 97% reduction in tracking error as compared to the uncompensated case. Furthermore, the IPMC’s position can be maintained for a period of 1200 seconds with minimal evidence of back relaxation. Furthermore, the control inputs in this case are bounded and significantly reduced, as compared to other control methods using unsectored IPMCs.

Dedication

For Mom and Dad.

Acknowledgements

I would first like to thank my advisor, Kam, for his guidance and support in this work.

I would like to thank Dr. Yantao Shen and Dr. Kwang Kim for serving on my thesis committee. I also thank Dr. Kim for access to the resources and personnel of his Active Materials and Processing Laboratory. I thank members of his research team, Viljar Palmre and David Pugal, for all the time spent fabricating IPMCs and offering insights into the project. I gratefully acknowledge financial support from the Office of Naval Research, grant number N000140910218.

I would like to thank my lab mates, Christopher Dudley, Joel Hubbard, M. Brandon Hurd, Norman Johnson, Brian Kenton, Dante Lorenzetti, Robert Riddle, and Yingfeng Shan. Thank you for all the time spent lifting me up, pointing me in the right direction, and making me laugh.

And finally I thank my family — Mom, Dad, Cory, and Natalie. Thank you for always believing in me, even at my worst.

Contents

1	Introduction	1
1.1	Importance	1
1.2	Contribution	2
1.3	Organization	3
2	Background	5
2.1	IPMC Mechanics	5
2.2	IPMC Application	9
2.3	Sectored IPMCs	13
2.4	IPMC Challenges	15
2.5	Alternative Actuators for Aqueous Applications	18
2.6	State-of-the-art Methods for Minimizing Back Relaxation	19
2.6.1	Manufacturing Approaches	20
2.6.2	Feedforward Control Approaches	21
2.6.3	Feedback Control Approaches	23
2.6.4	Integrated Feedforward and Feedback Control Approaches	25
2.6.5	Dual Input Single Output (DISO) Control Approaches	25
2.7	Summary	27
3	Modeling for Feedforward Control	30

3.1	Previously Used IPMC Models	30
3.2	Conventional Unsectored IPMC Model	34
3.3	A Secteded IPMC Model	37
3.4	Summary	38
4	Sector Control Strategy	40
4.1	Feedforward Control Approach	40
4.2	Adding Feedback Control	44
4.3	Summary	46
5	The Experimental System	47
5.1	IPMC Fabrication and Electrode Patterning	47
5.2	IPMC Test Setup	48
5.3	Model Validation	50
5.4	Summary	52
6	Experimental Results	53
6.1	Open Loop Response	53
6.2	Feedforward Control Response	54
6.3	Feedforward/Feedback Control Response	56
6.4	Alternative Waveforms	60
6.5	Summary	60
7	Conclusions	65
8	Future Work	67

List of Tables

5.1	Gain parameters for model validation.	50
6.1	Feedforward/feedback control results.	60

List of Figures

1.1	Concept: independently controlling each sector to produce a net canceling effect.	3
2.1	Chemical structure of Nafion [®] for IPMC fabrication [11].	6
2.2	IPMC cross section: (a) unactuated, (b) initial forward motion, and (c) back relaxation.	8
2.3	Typical unsectored IPMC in cantilever configuration with input voltage, $u(t)$, and output tip displacement, $y(t)$	9
2.4	IPMC open loop response to (a) step and (b) biased sinusoidal inputs.	10
2.5	Robotic fish with IPMC-based fins.	11
2.6	Finger with IPMC muscles in the joints [6].	12
2.7	Cardiac catheter guide wire, with an IPMC head.	13
2.8	IPMC electrode patterning techniques: (a) masking and (b) surface machining.	14
2.9	Unsectored and sectored IPMCs: (a) voltage applied across unsectored IPMC, (b) resulting bending motion, (c) opposing voltages applied to sectored IPMC, and (d) resulting twisting motion [9].	14
2.10	Block diagram showing general components of the IPMC response. . .	16

2.11	IPMC response when actuated underwater: (a) tip displacement frequency response showing dynamic effects, (b) varied responses to a constant step input, and (c) nonlinear trend of steady state current at different voltages.	17
2.12	General feedforward structure.	22
2.13	General feedback structure.	24
2.14	General integrated feedforward/feedback structures: (a) single loop and (b) double loop configurations [10, 43].	26
2.15	Disk drive control schemes: (a) master-slave, (b) PQ, and (c) decoupled architectures [44, 45].	28
3.1	Electromechanical IPMC input-output model, where the input voltage u is mapped to charge q , and then the charge produces curvature k	31
3.2	Clumped R-C model for IPMC electrical response [1, 46].	31
3.3	Distributed R-C model for IPMC electrical response [47–49].	32
3.4	R-C model used to describe electrical response [46].	35
3.5	Sector IPMC: (a) cantilever configuration with two inputs $u_1(t)$ (Sector 1) and $u_2(t)$ (Sector 2) and (b) the input-output model in the Laplace domain.	38
4.1	Feedforward control architecture for sector IPMC.	41
4.2	Simulated step responses of an IPMC’s total motion, forward motion component, and back relaxation component.	42
4.3	Block diagram of integrated feedforward/feedback control scheme.	45
5.1	Experimental setup for underwater actuation, including an IPMC with two effective sectors.	49
5.2	Simulink block diagram for feedforward tests.	50

5.3	Model validation: (a) input voltage for all tests, (b) individual and simultaneous sector actuation, (c) individual sector responses and corresponding simulation results, (d) simultaneous sector actuation and sum of corresponding simulations, and (e) error between simultaneous sector actuation and sum of corresponding simulations.	51
6.1	Open loop and feedforward responses to exponential reference: (a) tip displacement, (b) tracking error, and (c) feedforward input voltages.	55
6.2	Feedforward and feedforward/feedback responses to exponential reference: (a) tip displacement, (b) tracking error, and (c) input voltages.	57
6.3	Feedback response to exponential reference with input voltage threshold: (a) tip displacement and (b) input voltages.	58
6.4	Feedback response to exponential reference without input voltage threshold: (a) tip displacement and (b) power consumption.	59
6.5	Sectorized IPMC with a sinusoidal reference: (a) open loop and pure feedback control, and (b) feedforward and feedforward/feedback control.	61
6.6	Sectorized IPMC with a triangular reference: (a) open loop and pure feedback control, and (b) feedforward and feedforward/feedback control.	62
6.7	Sectorized IPMC with a trapezoidal reference: (a) open loop and pure feedback control, and (b) feedforward and feedforward/feedback control.	63
6.8	Sectorized IPMC with a twenty-minute exponential reference: (a) response and (b) input.	64

Chapter 1

Introduction

The goal of this thesis is to exploit the inherent characteristics of sectorized ionic polymer-metal composite (IPMC) actuators to mitigate the undesirable “back relaxation” effect they commonly exhibit. Existing methods to deal with back relaxation involve complicated fabrication processes and feedback control approaches which generate excessively high control voltages that can damage the IPMC. The aim of this work is to minimize relaxation without generating large control voltages and with only minimal additional fabrication beyond a standard process.

1.1 Importance

The IPMC material is a class of innovative electroactive polymer that offers combined sensing and actuating ability in a lightweight and flexible package. Setting IPMCs apart from other active materials are its soft and flexible structure, low driving voltage ($<5V$), and ability to operate in aqueous environments. These traits make IPMCs very attractive for underwater robotics [1–4]. Biomedical applications are also possible, including artificial muscles [5, 6] and endoscopy [7]. IPMCs are typically used in a simple cantilever configuration to create bending motion, however sectoring of the IPMC electrodes has been explored to alter the bending behavior. For instance, by applying different driving signals to different sectors of the IPMC, complex mo-

tion, specifically twisting, can be created [8, 9]. In certain applications, the benefits of IPMC actuators are overshadowed by unwanted dynamic effects and nonlinearities [10], the most obvious of which is back relaxation, which can cause significant positioning error when left uncompensated. When subjected to a DC input voltage, a Nafion[®]-based IPMC in the traditional cantilever configuration experiences a relatively quick deflection toward the anode side, followed by a slow period of relaxation toward the cathode side [11]. It is widely accepted that the so-called back relaxation effect is due to diffusion forces acting on the solvent within the ion exchange membrane. This effect can lead to significant positioning error and prevents it from being used in low-frequency applications. To name just a few examples, IPMCs have been suggested for use as pectoral fins on robotic fish for enhanced maneuverability [12], as artificial muscles [5, 6], or even as the head of a cardiac catheter [13]. In these and many other applications, low-frequency motions could be very common and would be adversely affected by back relaxation. Thus, minimizing or eliminating back relaxation is essential if IPMCs are to be used for many popular proposed applications. Furthermore, widely used performance-improving methods, such as feedback control, demand a large input voltage, which can also limit the practical use of IPMCs, especially in biomedical applications where any increase in voltage amounts to a decrease in safety. With this consideration, it is also important to decrease the voltage demand, as compared to existing feedback techniques.

1.2 Contribution

The contribution of this work is a new method to mitigate back relaxation, utilizing sectorized IPMCs. The new method described herein involves driving different sectors of the IPMC in opposing directions, essentially canceling out the back relaxation. Figure 1.1 illustrates the basic concept, displaying the relaxation experienced by each

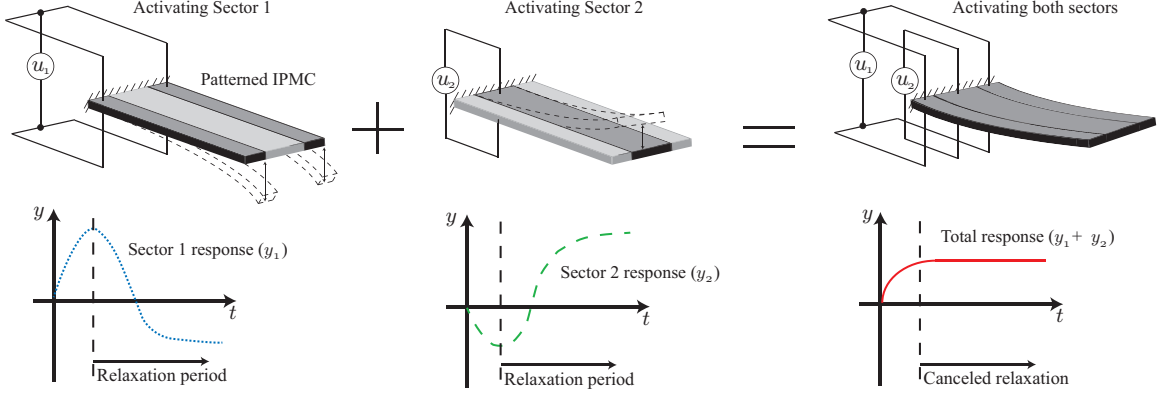


Figure 1.1: Concept: independently controlling each sector to produce a net canceling effect.

sector when supplied with opposing inputs (u_1 and u_2), and the net canceling effect. A patterning technique and model-based feedforward controller are developed based on this principle, and are shown to significantly reduce tracking error due to back relaxation, improving the tracking error of a steady reference trajectory by approximately 85%. To further improve the response, feedback control is integrated with the feedforward controller to account for nonlinearities, disturbances, and other undesirable behaviors not captured in the model. The integrated feedforward/feedback control method brings the tracking error improvement to nearly 97%, while significantly reducing the required input voltage, as compared to the pure feedback case.

1.3 Organization

This thesis is organized as follows. Chapter 2 provides background information on the problem at hand. The fundamental mechanisms governing IPMC motion are described. Popular applications and the associated challenges are presented, as well as past work to improve the IPMC response (particularly back relaxation), including material and control methods. Pertinent control methods for systems other than

IPMCs are also discussed. Modeling is discussed in Chapter 3. Previously used IPMC models are discussed in detail, followed by the model used in this work for both traditional and sectored IPMCs. Chapter 4 presents the control techniques implemented in this work, starting with a pure feedforward approach, and then adding in feedback control. The experimental system is discussed in Chapter 5. The IPMC fabrication procedure is included, as well as a description of the test setup and all the key pieces of equipment that were used. Experiments are also presented here which were used to validate the modeling techniques. Experimental results are given in Chapter 6, demonstrating the effectiveness of the developed control techniques. Finally, concluding remarks are made in Chapter 7, and suggestions for future work are given in Chapter 8.

Chapter 2

Background

This chapter serves to provide background on ionic polymer-metal composites (IPMCs). First, the structure is described, as well as the mechanism for actuation and back relaxation. A few representative application examples are then discussed. Next, segmented IPMCs are introduced, followed by some of the larger challenges associated with application of IPMCs. The benefits of IPMCs over several other means of actuation are discussed. Finally, techniques previously used to improve the IPMC actuation response are reviewed. Included are fabrication and control methods, including control methods for other dual input single output (DISO) systems for completeness.

2.1 IPMC Mechanics

An IPMC actuator consists of an ion exchange membrane, plated on both sides with a noble metal, to serve as electrodes. Platinum or gold is typically used for the electrodes. In most cases, the membrane used is Nafion[®], a perfluorosulfonic acid polymer with a fixed sulfonate anion, as shown in Fig. 2.1. Paired with the sulfonate groups are some kind of mobile cation, often sodium or lithium [see Fig. 2.2(a)] [11,14].

There are differing theories behind the mechanism of actuation, but it is known that when a constant voltage is applied across the hydrated membrane (via the electrodes), there is a quick deflection of the actuator toward the anode, and if the voltage

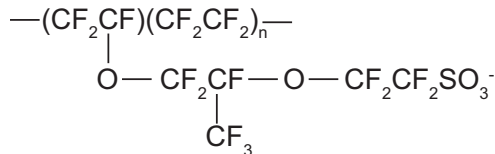


Figure 2.1: Chemical structure of Nafion[®] for IPMC fabrication [11].

is held long enough, the IPMC will experience a back relaxation, moving toward the original position [11]. It is widely accepted that the initial application of an electric field creates a charge on the electrode surface, which attracts the mobile cations toward the cathode. The cations are bonded to water molecules, which are also transported through the membrane. In [11], it is proposed that the initial bending is caused by the additional cations drawn to the cathode. It is suggested that these cations repel the cation-anion pseudo-dipoles already present in the region, causing expansion on this side of the membrane. Then, the cations slowly diffuse away from the cathode, affected by the sulfonate groups, and this causes relaxation. A more prevalent theory is that the abundance of water molecules near the cathode causes swelling of the membrane on this side, and results in bending toward the anode [see Fig. 2.2(b)]. Then, relaxation is caused by the migration of water molecules back toward the anode side, due to diffusion forces. In some cases, it has been suggested that it is loose water molecules (not bonded to cations), that diffuse back toward the anode to produce back relaxation [15, 16]. In [17], a similar explanation was given in which water molecules in the cathode break free of their bonds to cations after prolonged exposure to an electric field, and subsequently migrate back toward the anode. It has also been suggested that the bonded cations and water molecules diffuse back through the membrane together, as shown in Fig. 2.2(c) [18]. It would be difficult to measure the individual forces acting on the cations and water molecules inside, but

a very simple estimate can be made using the following relationship:

$$F = Eq, \quad (2.1)$$

where F is the force acting on a particle of charge q in an electric field of strength E . If the cation is a sodium ion (Na^+) with a charge equal to the elementary charge ($e = 1.602 \times 10^{-19}$ C) and the electric field is assumed constant and uniform throughout the IPMC, then 1.5 V applied across the electrodes (500 μm apart) would yield a force of $F = (1.5 \text{ V}/0.0005 \text{ m})(1.602 \times 10^{-19} \text{ C}) = 4.806 \times 10^{-16}$ N on each cation after the electrodes are fully charged. Further, if we assume a cation concentration of $C_0 = 10^{-4}$ mol/ m^3 [19] and use the IPMC volume of $V = (0.05 \times 0.01 \times 0.0005) \text{ m}^3 = 2.5 \times 10^{-7} \text{ m}^3$, then the summed charge of all the cations would be $q_{tot} = VC_0eA = 2.411 \times 10^{-6}$ C, where $A = 6.02 \times 10^{23}$ atoms/mol is Avogadro's number. Using this charge in Eq. 2.1, the total distributed electrostatic force on the cations within the IPMC is $F = (1.5 \text{ V}/0.0005 \text{ m})(2.411 \times 10^{-6} \text{ C}) = 7.233 \times 10^{-3}$ N. As described further in Chapter 3, in this work, the motion of the IPMC is assumed to stop when the electrostatic forces and diffusion forces are in balance, meaning the total distributed diffusion force acting on the water molecules bonded to the cations would be equal and opposite to the electrostatic force at steady state.

In this work and in many other settings, the IPMCs are used in a cantilever configuration as shown in Fig. 2.3. Here, an input voltage, $u(t)$, is applied to produce some tip displacement, $y(t)$. Figure 2.4(a) shows the tip deflection for a typical IPMC step response from this configuration. As described previously, there is a relatively quick forward motion, followed by a slow period of relaxation. However, relaxation is not only present when subjected to step inputs. As long as the input signal has low enough frequency content, back relaxation will set in. For example, a sine wave of sufficiently high frequency would not induce relaxation, but if it were biased, the

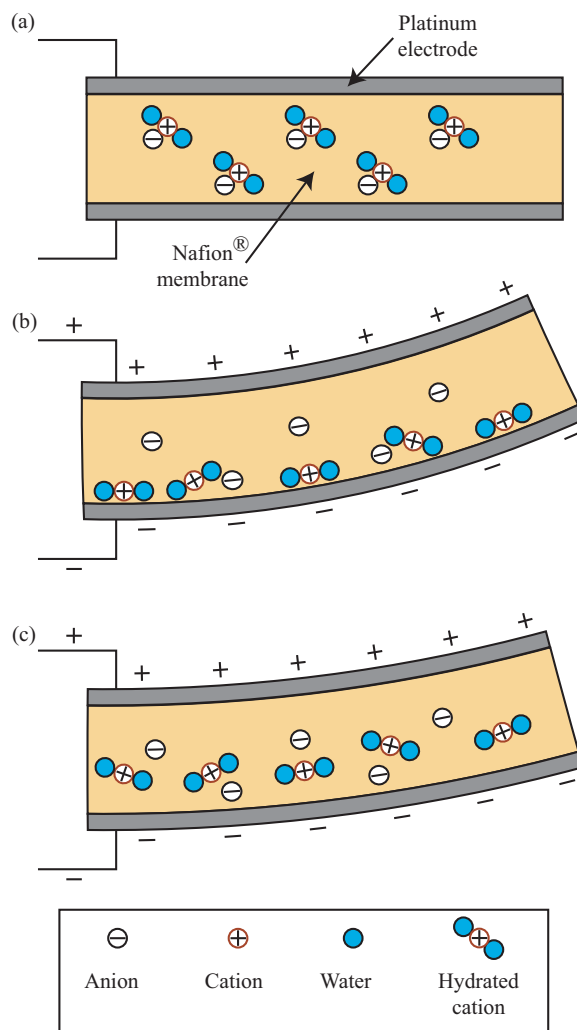


Figure 2.2: IPMC cross section: (a) unactuated, (b) initial forward motion, and (c) back relaxation.

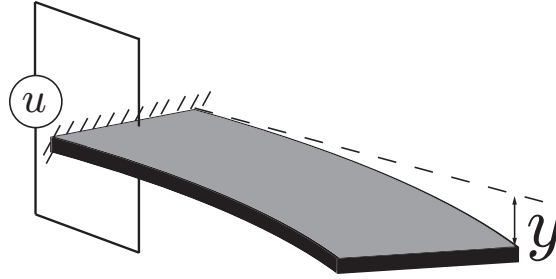


Figure 2.3: Typical unsectored IPMC in cantilever configuration with input voltage, $u(t)$, and output tip displacement, $y(t)$.

DC component of the signal would cause relaxation, as shown in Fig. 2.4(b).

The relationship between relaxation and humidity has been extensively studied. It has been shown that when operated in an increasingly more humid environment, the IPMC's stiffness decreases, and the level of relaxation increases, as does the initial forward movement [20, 21]. This implies that if an IPMC were operated in air rather than water, the level of relaxation would decrease over time, as the actuator became more dehydrated. Unfortunately, the forward movement would also decrease over time until eventually the actuator was completely dried and there would be virtually no motion. It could be argued that there is an ideal humidity, striking a balance between forward motion and relaxation. This would require a humidity-controlled environment, however, which is not realistic for most practical applications.

2.2 IPMC Application

One of the largest areas of interest in IPMC application is the field of underwater robotics. Since they are able to operate silently in aqueous environments, they can be very useful for propulsion and maneuvering of underwater vehicles, especially those that are bio-inspired. Various aquatic animals have been mimicked, including the tadpole [22], jellyfish [23, 24], manta ray [25], and simple fish [3, 26]. Most swimming

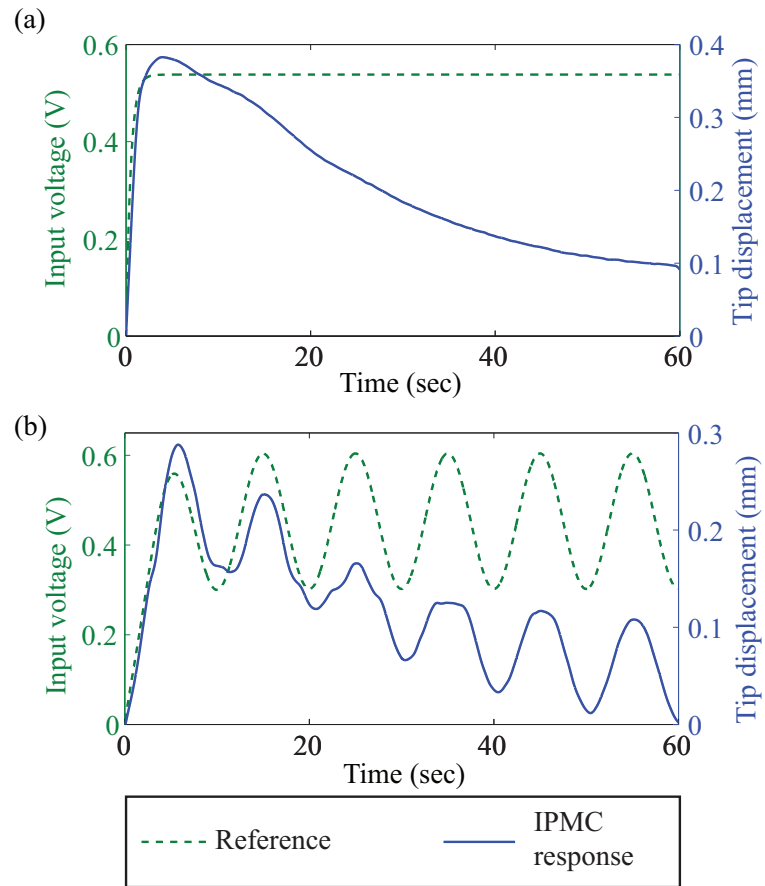


Figure 2.4: IPMC open loop response to (a) step and (b) biased sinusoidal inputs.

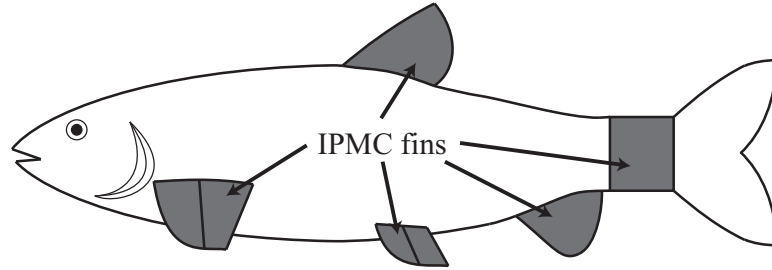


Figure 2.5: Robotic fish with IPMC-based fins.

robots have only a caudal (tail) fin to produce both propulsion and maneuvering, either altering the duty cycle or biasing the input voltage to induce turning [22, 27]. Monolithic IPMCs capable of complex deformation have also been created for use as pectoral fins to allow for enhanced maneuverability [12, 28]. Theoretically, any number of IPMC fins could be added to create a more maneuverable swimming robot (see Fig. 2.5).

Due to their flexibility and low driving voltage, IPMCs have also gained much attention for their potential to be used as “artificial muscles” in medical applications. For example, they have been suggested for use as cardiac-assist muscles, helping to regulate the beating of an ailing heart [6]. It has also been proposed to use IPMCs in the creation of a complete hand prosthesis [5], or as additional muscles in finger joints, used to assist with movement (see Fig. 2.6) [6].

Surgical tools can also be improved using IPMCs. Several tools designed for minimally invasive surgery have room for improvement with IPMCs. Traditionally, these small instruments have complex mechanical linkages which are used to guide the tool. If an IPMC were used for guidance, however, the linkage could be removed, reducing the size of the instrument and the necessary incision in the patient. Examples of such tools include a gripping tool, used for object manipulation during surgery [29], an endoscope, used for internal imaging [7], and a cardiac catheter [13]. Rod-shaped IPMCs, capable of three dimensional motion have also been created, and would be

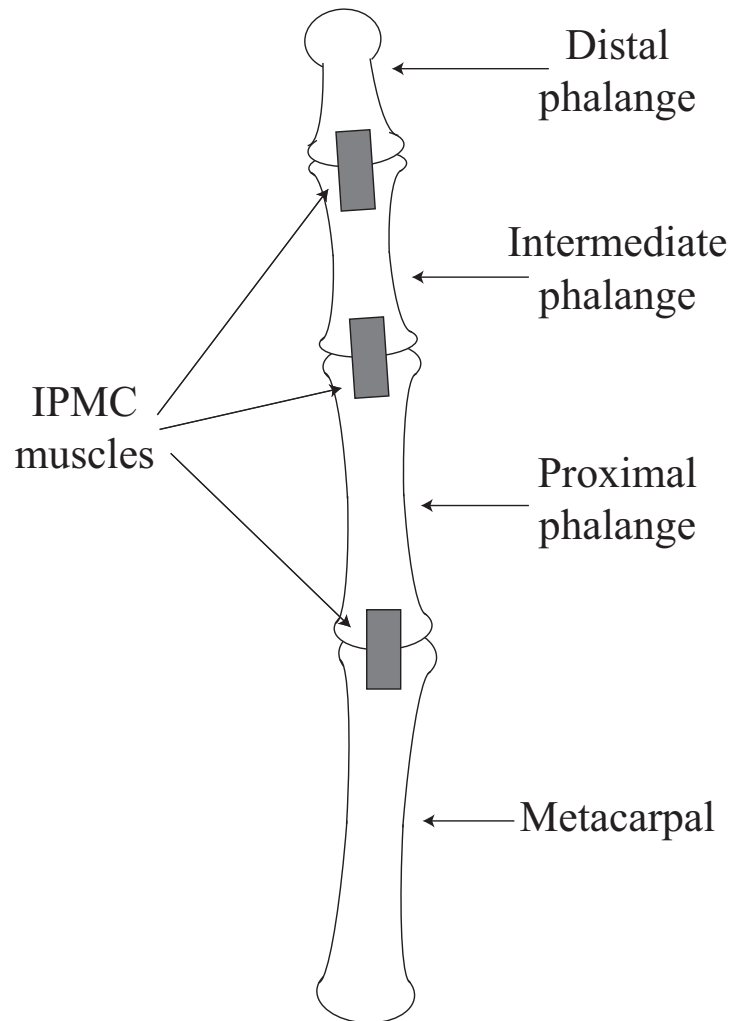


Figure 2.6: Finger with IPMC muscles in the joints [6].

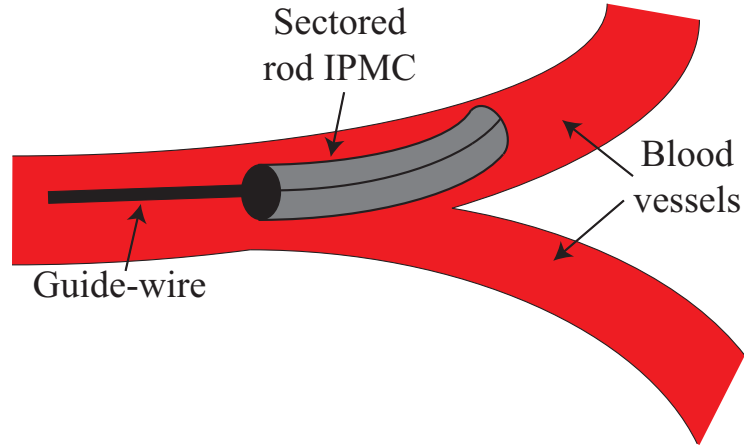


Figure 2.7: Cardiac catheter guide wire, with an IPMC head.

helpful for these applications (see Fig. 2.7) [6].

2.3 Sectored IPMCs

The range of capabilities of IPMCs can be expanded by sectoring (patterning) the IPMC's metal surface into several electrically isolated portions. There are several methods used to accomplish this, including masking of the Nafion[®] during plating [see Fig. 2.8(a)], or cutting the complete platinum surface using a CNC machine, laser, or even a sharp blade [see Fig. 2.8(b)] [9, 30, 31]. In this configuration, different voltages can be applied to different sectors to produce complex motion [8, 9, 30]. For example, if opposite voltages were applied to a two-sectored IPMC, the sectors would bend in opposite directions and produce a twisting motion, as illustrated in Fig. 2.9. In addition to actuation, IPMCs also have the ability to sense motion, producing a voltage when subjected to a deflection. With a sectored IPMC, an integrated actuator/sensor can be developed using part of the IPMC to produce motion and another part to sense this motion [31, 32].

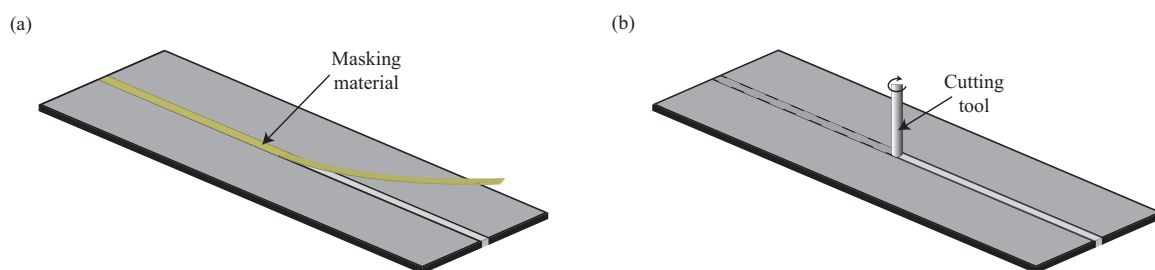


Figure 2.8: IPMC electrode patterning techniques: (a) masking and (b) surface machining.

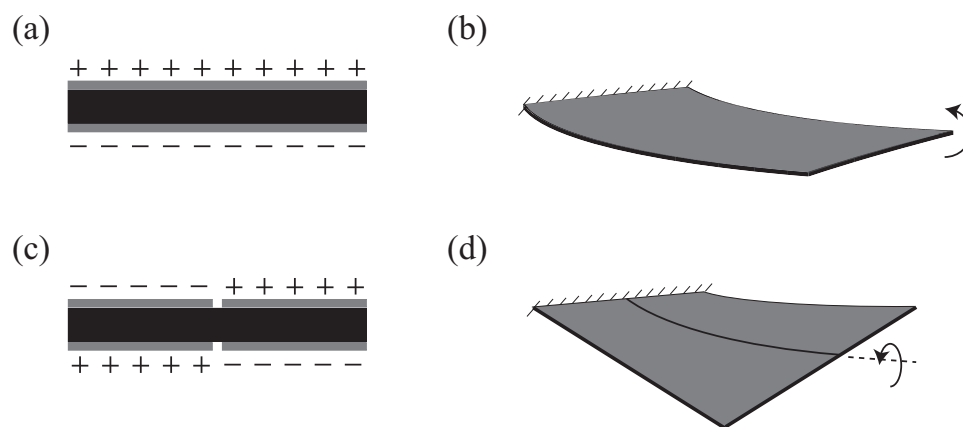


Figure 2.9: Unsectored and sectored IPMCs: (a) voltage applied across unsectored IPMC, (b) resulting bending motion, (c) opposing voltages applied to sectored IPMC, and (d) resulting twisting motion [9].

2.4 IPMC Challenges

Although this work focuses on the correction of back relaxation, there are other large challenges to the application of IPMCs that will be described for completeness. These challenges can be seen in the response of a typical unsectored IPMC actuated underwater in a cantilever configuration, when an input voltage is supplied and the tip displacement is measured with a laser displacement sensor (see Fig. 2.3). A block diagram is given in Fig. 2.10 to illustrate these issues. In this representation, the system input, u , is summed with any input disturbances, d_1 , and fed into H , which dictates the electrical response. H is dependent on the frequency of the input and also has a nonlinear dependence on the input amplitude. G_F and G_B represent the high-frequency dynamic effects, related to the forward motion, and the low-frequency back relaxation behavior, respectively. Both of these are dependent on frequency as well as time. These responses are summed with the external disturbances, d_2 , to yield the system output, tip displacement, y . A sample IPMC frequency response is given in Fig. 2.11(a). On a relatively high frequency range, the IPMC shows a typical second order response, including a resonance, after which the magnitude of the output is decreased and the phase experiences a large shift. Dynamic effects necessitate some form of control for most applications. The time-varying behavior and nonrepeatability of the dynamic effects and back relaxation lead to discrepancies between IPMC responses to the same input [see Fig. 2.11(b)] and make any control effort (especially model based control) somewhat more difficult. The primary source of nonlinearity in an IPMC is the electrical response. The current flowing through the actuator is nonlinearly dependent on the input voltage. For instance, even over a relatively low voltage range the steady state current of the IPMC shows a very nonlinear trend [see Fig. 2.11(c)]. This nonlinearity is propagated through the rest of the response to produce nonlinear tip displacements. Nonlinearity can also make the

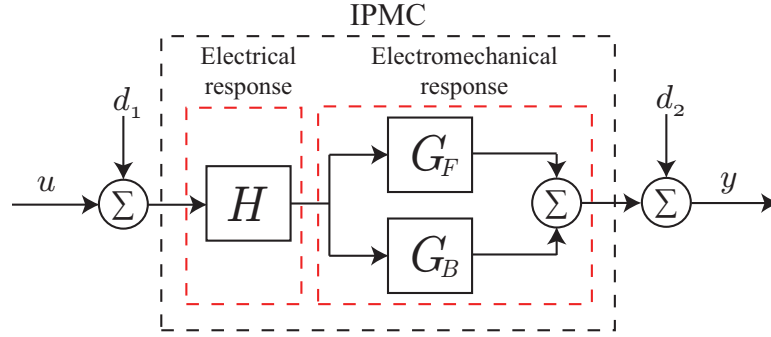


Figure 2.10: Block diagram showing general components of the IPMC response.

modeling process more difficult [33]. While any of these problems can adversely affect the previously discussed applications, back relaxation is studied in this work simply because there isn't an effective method to compensate for it without unnecessary fabrication steps or control schemes with excessively high input demands.

In the case of underwater robotics, back relaxation can limit maneuverability. If the goal was to have an underwater robot (like that shown in Fig. 2.5) swim straight forward, the IPMC-based caudal fin would be flapped in a periodic motion relatively quickly, and back relaxation would not be a significant factor. However, any other kind of maneuvering could require a signal with low frequency components, which would induce back relaxation. As previously described, a biased input voltage can be supplied to the caudal fin to induce turning by flapping the fin about a non-neutral axis. There is a DC component to the input signal to create the bias, and this would lead to relaxation. If the turn lasted long enough, the caudal fin might relax enough to compromise the maneuver. Similarly, if pectoral fins were used for turning, or any other slow maneuver (i.e., diving, rolling), relaxation could seriously hurt performance. Artificial muscle applications also suffer because of back relaxation. In the example of the hand prosthesis, quick movements might not be particularly problematic. Any static tasks (like holding an object), however, could induce back relaxation and cause the subject to lose the grip. Medical applications bring extra at-

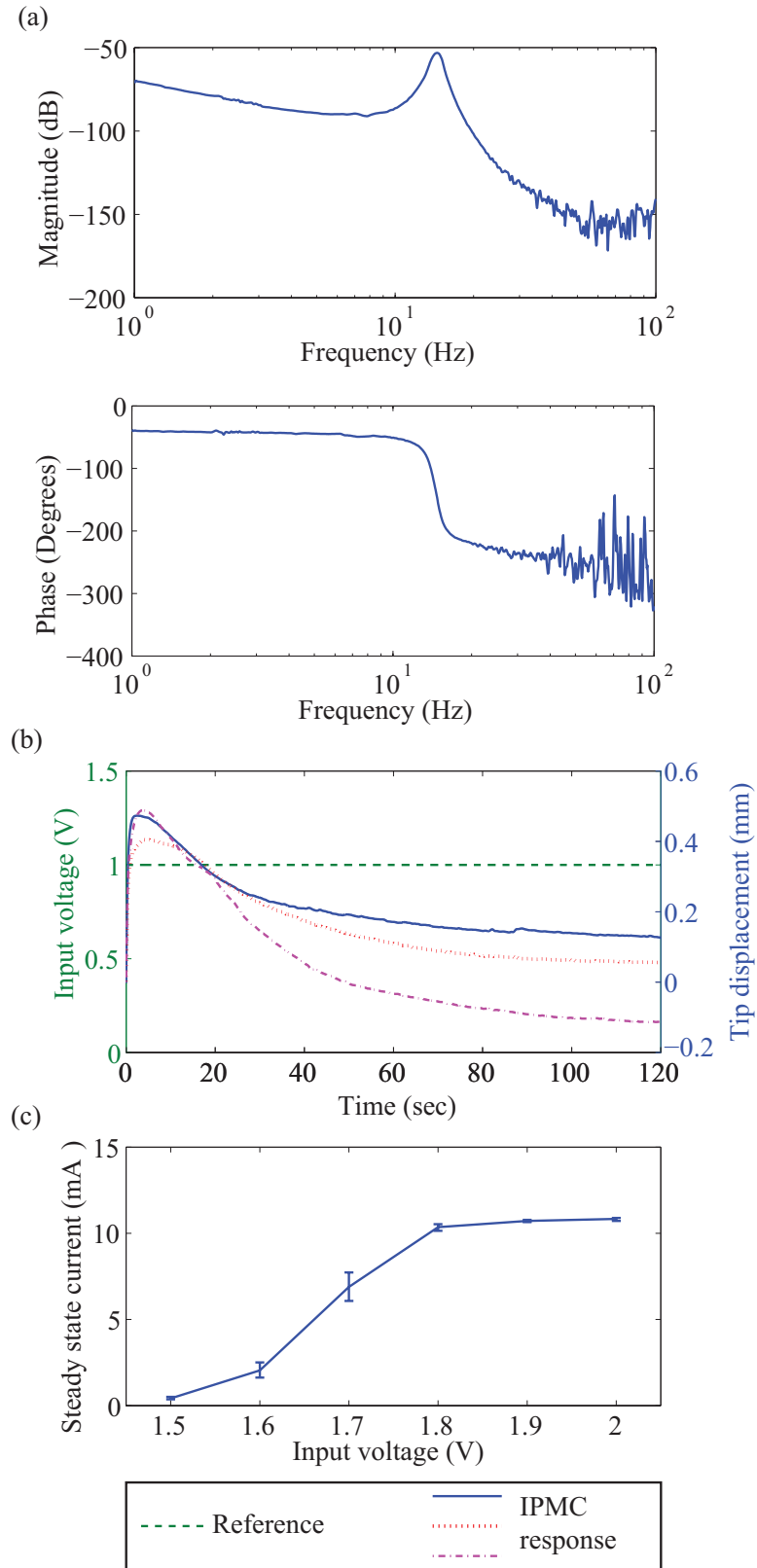


Figure 2.11: IPMC response when actuated underwater: (a) tip displacement frequency response showing dynamic effects, (b) varied responses to a constant step input, and (c) nonlinear trend of steady state current at different voltages.

tention to the safety issues back relaxation can cause. In the example of the catheter, the significance of back relaxation is obvious. Any slow movements of the IPMC (which are likely) could easily induce back relaxation. Since the IPMC is used here to guide a catheter through blood vessels to the heart, any tracking error could send the catheter in the wrong direction, potentially making the operation a failure and seriously injuring the patient.

2.5 Alternative Actuators for Aqueous Applications

There are, of course, many alternatives to IPMCs for actuation, and serious consideration must be given to the pros and cons of each before deciding an IPMC is fit for a given application. Many functions performed by an IPMC can be replicated more efficiently using an electric motor. For instance, sectored IPMCs can be used to twist and produce a torque. In terms of torque-to-weight ratio, a 1-mm thick IPMC is comparable to a small DC motor (no gearbox), however a hobby servo motor can show nearly an order of magnitude improvement in this ratio [9]. In this instance, the advantage of an IPMC is the ability to be scaled down. Having no internal moving parts, an IPMC can be easily reduced to a smaller size, whereas it becomes increasingly more difficult to manufacture a motor at smaller sizes. This issue is compounded when complex motions are needed. For a motor to produce motions beyond simple twisting, intricate linkages sometimes must be developed, making it even more difficult to scale this technology down. As a generality, motors can also produce a significant amount of noise, which is especially undesirable for underwater applications.

The issue of compactness is avoided with most active materials. Piezoelectric

materials, for instance, can show tremendous performance, even at a very small size. Compared to an IPMC, a piezoelectric material can produce a much higher force and has a greater operating bandwidth. In terms of displacement that can be achieved, IPMCs are far superior. Although the displacement from an IPMC comes in the form of bending, rather than axially like a piezoelectric, the strain realized for an IPMC ($\sim 10\%$) is much greater than that of a piezoelectric ($0.1-0.3\%$). While IPMCs require voltages typically less than 5V to operate, typical piezoelectric applications require voltages in excess of 100V [34,35], which make piezoelectrics undesirable for any kind of medical application. Also popular are shape memory alloys (SMAs). SMAs can take many different shapes and configurations, however, they are commonly setup in a spring shape, allowing for axial motion. In this configuration, the necessary voltage is comparable to that of an IPMC, and a greater force can be produced. The strain produced is also significantly greater ($\sim 30\%$). The main drawback, however, is the speed. It takes a relatively long time for the material to regain its shape, giving it a lower bandwidth than an IPMC [35].

2.6 State-of-the-art Methods for Minimizing Back Relaxation

In the literature, many approaches have been proposed to address the back relaxation effect. Most solutions are either material/fabrication methods or control methods. In this work, it is desired to employ a method that does not involve much deviation from a standard fabrication approach, like that given in [14]. Material/fabrication methods will still be discussed for completeness, however.

2.6.1 Manufacturing Approaches

One approach to mitigate back relaxation is to use a different polymer membrane, such as Flemion. Flemion is similar in structure to Nafion[®], although the anions fixed to the polymer backbone in this case are carboxylates, rather than sulfonates. As with Nafion[®], a Flemion-based IPMC experiences a fast deflection towards the anode when a DC voltage is applied. After this, however, a Flemion-based actuator slowly continues to bend in the same direction [11]. Of suitable membranes for IPMCs, however, Nafion[®] is the most commercially available, making it the material of choice.

The effect of solvents has also been explored, and it has been shown that the proper combination of solvent and cation can eliminate back relaxation. For instance, Nemat-Nasser and Zamani showed that back relaxation is not present for a Nafion[®]-based IPMC with potassium cations and a crown ether (18-Crown-6) as the solvent. The forward motion, however, was significantly slowed down, taking over 11 min to reach its full forward position [36]. Perhaps a larger problem is that most practical IPMC applications would require that the actuator be immersed in water, meaning the IPMC would have to be sealed to retain a different solvent. A silicone coating was used to seal water in an IPMC in [37]. The coating was successful for four months, and could likely be used to seal in an alternative solvent as well, but this is still an undesirable solution, as it necessitates a significant extra step in fabrication, and could stiffen the actuator.

Different electrode development processes have also been shown to help reduce back relaxation. The insertion of a palladium buffer between the ion exchange membrane and platinum was studied in [18]. It was shown that the palladium layer created a more solid first electrode layer, compared to platinum which tends to break up into clusters. Once the first layer is in place, platinum can be more effectively applied on top. In [38], different alcohols were used in place of water as the medium for plat-

inum reduction. It was shown that using ethanol instead of water produces a thicker platinum layer, most likely due to increased swelling of the membrane during plating. Both of these methods showed a reduction in back relaxation, however fabrication is further complicated with either approach.

2.6.2 Feedforward Control Approaches

Alternative to material alterations, many control methods have been implemented to improve the response of IPMCs made in a traditional manner. Unfortunately, most control methods produce a steadily increasing input voltage to the IMPC. This is undesirable primarily because a voltage threshold will eventually be crossed at which the solvent in the actuator will undergo electrolysis. As this can permanently damage the actuator, it is best to keep the input below the electrolysis point. The typical potential associated with electrolysis of water at 25°C and a neutral pH is 1.23 V. For IPMCs, however, this potential might be larger, as dictated by the experimental conditions and material properties. In [39] the electrolysis potential for an IPMC was identified as 1.8 V. Past this point the resulting reaction splits water into hydrogen and oxygen and results in a higher current draw than is necessary for IPMC actuation. This is essentially wasted current, and leads to inefficient actuation. The degree to which electrolysis occurs in the actuation cycle is determined by the magnitude of the applied voltage and the shape or dynamic properties of the input. Increased input voltage also undermines one of the most attractive qualities of the IPMC: low driving voltage. Greater input voltages lead to unnecessary power consumption and greater risk of damage of both the actuator and the surrounding environment, especially in biomedical applications.

Feedforward control has been used in several cases to improve IPMC performance. Feedforward is an open-loop and often model-based method, not relying on any feed-

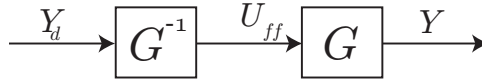


Figure 2.12: General feedforward structure.

back, but instead predicting the response of the system. In its simplest form, a model of the plant, $G(s)$, is inverted to create a controller, $G^{-1}(s)$, as shown in Fig. 2.12. The feedforward input to the system, $U_{ff}(s)$, is then given as

$$U_{ff}(s) = Y_d(s)G^{-1}(s), \quad (2.2)$$

and therefore

$$Y(s) = U_{ff}(s)G(s) = Y_d(s), \quad (2.3)$$

indicating theoretically perfect tracking between the output, $Y(s)$, and the reference, $Y_d(s)$. Feedforward can be very effective if a very accurate model is used, however it is not typically robust when disturbances are introduced. It should be noted, however, that if the feedforward input comes from the inverse model of the relaxing system, it will compensate by ramping up to excessively high values. A dynamic model was inverted and used for feedforward control in [10], significantly improving the tracking error under a periodic reference. In this example, however, feedforward control was studied for use in a relatively high frequency regime, for which back relaxation is not a large factor. Feedforward can also be used to address just part of the plant model. Although it was not used to remedy back relaxation, a good example of inversion-based feedforward is given in [16], in which feedforward control was used to eliminate the hysteresis experienced by IPMCs. The hysteresis effect was modeled and inverted to produce the control input to the IPMC.

2.6.3 Feedback Control Approaches

Sensor-based feedback control can be used to create a more robust closed-loop system, better equipped to handle disturbances (see Fig. 2.13). In this case, the control input from the feedback controller, $C_{fb}(s)$, is based on the tracking error, $E(s)$:

$$U_{fb}(s) = C_{fb}(s)[Y_d(s) - Y(s)] = C_{fb}(s)E(s). \quad (2.4)$$

The closed-loop transfer function is given as

$$\frac{Y(s)}{Y_d(s)} = \frac{C_{fb}(s)G(s)}{1 + C_{fb}(s)G(s)}. \quad (2.5)$$

Feedback control has been used much more widely than feedforward control to improve the response to both DC and dynamic references. Although it doesn't provide the theoretically perfect response of a feedforward controller, it is typically more robust to unmodeled effects and outside disturbances. A representative example is given in [40], in which the authors developed a lead-lag feedback compensator to maintain the position of an IPMC. The compensator significantly reduced the overshoot and settling time for the system's step response. While this method is effective and easy to implement, the control input generated by the compensator tends to ramp up quickly in order to prevent back relaxation. In [41], a linear quadratic regulator (LQR) feedback controller was developed, to minimize settling time while constraining the input voltage by using a cost function of the form

$$V = \int_0^{\infty} [x'(t)Q(t)x(t) + u'(t)R(t)u(t)]dt, \quad (2.6)$$

where $x(t)$ is the state vector, $u(t)$ is the control input, and $Q(t)$ and $R(t)$ are their respective weighting matrices. This significantly improved the response, but only a

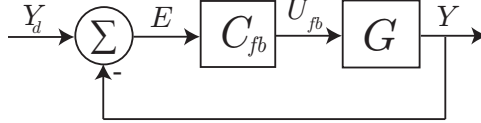


Figure 2.13: General feedback structure.

short testing time is demonstrated (less than 30 seconds). For this period of time, back relaxation would not necessarily be a large factor, and would become more significant as time went on. In [42], robust control techniques (H_∞ , H_∞ with loop shaping, and μ -synthesis) were employed to improve the time response, especially as it is affected by non-repeatability and uncertainty in the IPMC performance. These controllers are all based on the idea of minimizing the H_∞ norm of the closed-loop transfer function, $T(s)$. The norm represents the largest possible gain of the system over the considered frequency range, and is given as

$$\|T(s)\|_\infty = \max_{\omega} |T(j\omega)|. \quad (2.7)$$

These controllers all have benefits, and μ -synthesis specifically can yield a steady response under a very low control input. However, the response is again only demonstrated for a very short period of time, in which back relaxation may not be a large concern. One of the very few available control methods designed specifically for a sectored IPMC is given in [30]. Here, a feedback controller is designed (but not fully implemented) using the inverse Jacobian of the IPMC motion, as it fits into a multilink kinematic model of the sectored IPMC. A visual sensing system is used to monitor the movement of several points on the IPMC. This sort of sensing is effective if complex motion is important to the application. In this work, however, simple bending is the desired behavior, so multilink modeling would be superfluous.

2.6.4 Integrated Feedforward and Feedback Control Approaches

Integrated feedforward and feedback schemes have also been implemented to tackle different aspects of the control issues with different controllers. In [43], the model of the IPMC was separated into three components, a time delay, a linear transfer function, and a nonlinear gain. The nonlinear component was inverted and used as a feedforward controller to remove the nonlinear behavior. A feedback controller is then added to improve the response of the “linearized” system. In this case, a single loop is used, in which the feedback input, $U_{fb}(s)$ is fed into the feedforward controller to produce the feedforward input, $U_{ff}(s)$. This method was shown to improve the response to both DC and dynamic references, but control inputs are not given to indicate any boundaries. A generalized version of this configuration, inverting the entire plant for the feedforward controller, is given in Fig. 2.14(a). In [10], a feedback controller, designed to compensate for effects not captured in the model used, was added to the previously described feedforward controller, designed to compensate for dynamic effects. In this case, the feedforward and feedback controllers were kept on separate loops of the control structure, and the feedforward and feedback inputs were added to produce a total control input, $U(s)$. With this configuration either component could be shut off and the system would still be functional. The architecture is similar to that shown in Fig. 2.14(b). The performance was further improved with the addition of feedback, however the compensators were designed for relatively high frequency references, for which relaxation is not significant.

2.6.5 Dual Input Single Output (DISO) Control Approaches

A general patterned IPMC under simple bending, with any number of sectors, can be considered a multiple input single output (MISO) system, meaning that there is an input for each sector, but only a single output (tip deflection in this case). In

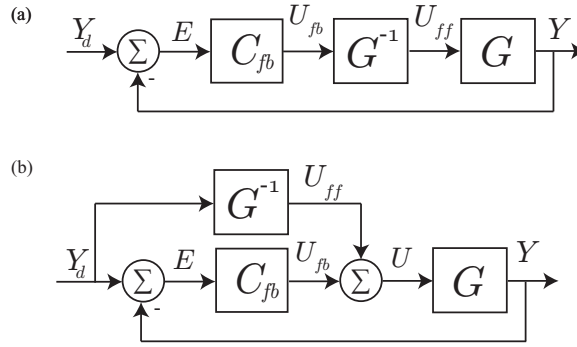


Figure 2.14: General integrated feedforward/feedback structures: (a) single loop and (b) double loop configurations [10, 43].

this work, the IPMCs used only had two sectors, and were thus considered to be dual input single output (DISO) systems. Since there has not been much work in the control of sectored IPMCs, control strategies for other DISO systems were studied. One of the most studied DISO systems in the literature is the hard disk drive. To cover a large area quickly and precisely, the read/write head often has both a coarse and fine actuator, for instance a voice coil motor and a piezoelectric microactuator. One general control architecture is the “master-slave” method [see Fig. 2.15(a)]. This relies heavily on the assumption that there is minimal interaction between the two actuators (they are essentially decoupled). The “master” controller, $C_1(s)$, provides the input to the fine actuator, $G_1(s)$, as well as the reference input to the “slave” controller, $C_2(s)$, which produces the input for the coarse actuator, $G_2(s)$. The closed-loop transfer function of such a system is very similar to that of the general feedback system (see Eq. 2.5), but is complicated somewhat by the addition of the second actuator:

$$\frac{Y(s)}{Y_d(s)} = \frac{C_1(s)[G_1(s) + C_2(s)G_2(s)]}{1 + C_1(s)[G_1(s) + C_2(s)G_2(s)]}. \quad (2.8)$$

The primary source of failure for this method is excessive interaction between the actuators, making the decoupled assumption invalid. Alternative to this method is the “PQ” method [see Fig. 2.15(b)]. Here, individual and independent controllers are

assigned to each actuator to produce stable zeros for the parallel system. To achieve this, the controllers must be selected to fit the following relation:

$$1 + \frac{G_2(s)C_2(s)}{G_1(s)C_2(s)} = 1 + PQ = 0, \quad (2.9)$$

where $P = \frac{G_2(s)}{G_1(s)}$ and $Q = \frac{C_2(s)}{C_1(s)}$. Then a feedback loop and an additional controller, $C_0(s)$, are designed to improve the response of the actuators and previously designed compensators, which are now treated as a single input single output (SISO) system. This method is well suited to systems in which the two plants have distinct, different bandwidths, so the frequency content of a reference can be properly divided amongst the actuators [44]. A “decoupled” architecture for a disk drive system is presented in [45] [see Fig. 2.15(c)]. Otherwise similar to the PQ method, here the output of the fine actuator is estimated with a model and then subtracted from the total measured output, to produce the estimated output of the coarse actuator. This allows the error fed to the coarse actuator’s compensator to be more accurate, without actually measuring individual outputs of each actuator. Inaccuracy of the extra model used for estimation can lead to failure of this control architecture, as can excessive coupling between actuators, as described for master-slave control.

2.7 Summary

IPMCs could be used advantageously for many applications, however back relaxation stands in the way of realizing some of these applications. There are a great number of methods to improve the response of IPMCs, and most can be applied to reduce or even eliminate back relaxation. Adjustments to the fabrication technique have been shown to be effective, however most methods are either impractical for real world applications or make the fabrication process undesirably complex. Feedforward,

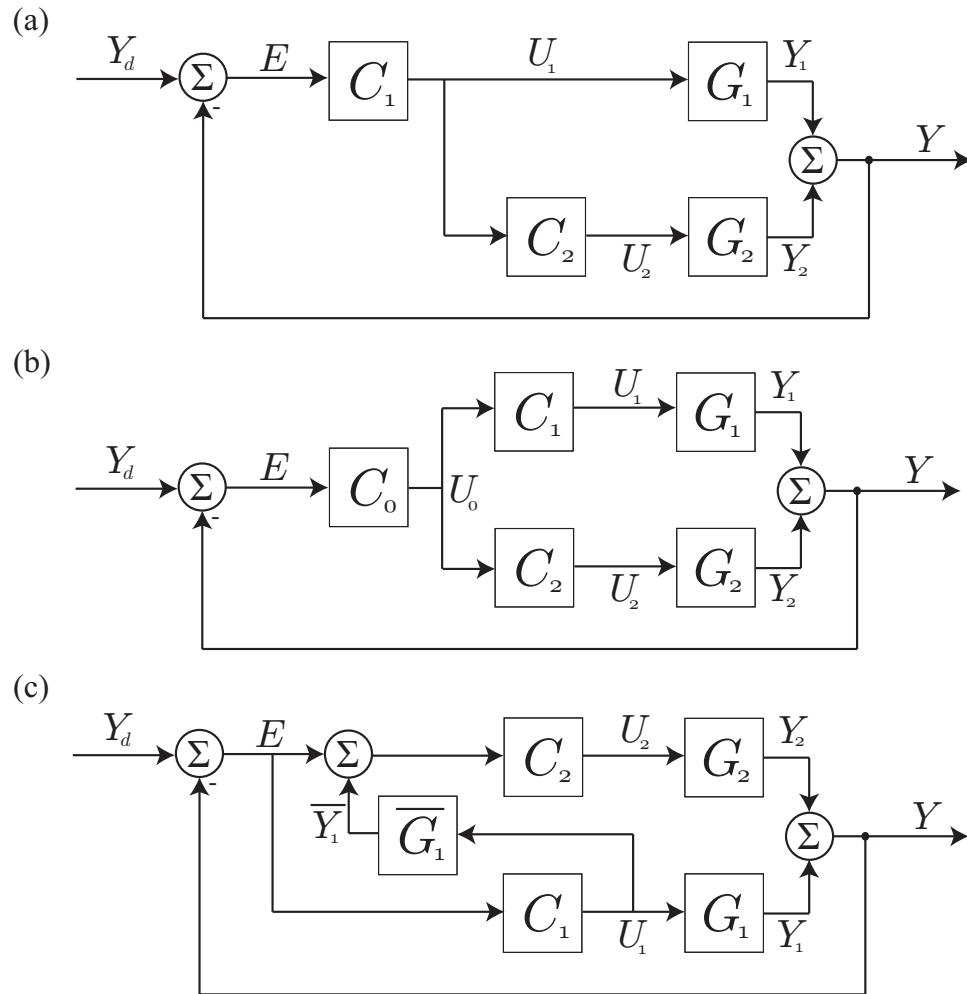


Figure 2.15: Disk drive control schemes: (a) master-slave, (b) PQ, and (c) decoupled architectures [44, 45].

feedback, and integrated feedforward/feedback control methods can also be used to correct back relaxation, although no method has been shown to effectively bound the control input voltage without compromising the actuation behavior. Little work has been done in the area of controlling the sectored IPMC as a DISO system, so control methods developed for other DISO systems, such as the hard disk drive, can be used as a starting point.

Chapter 3

Modeling for Feedforward Control

In this chapter, several existing IPMC electrical and electromechanical models are presented. Modeling is not absolutely necessary for all methods to mitigate relaxation. In this work, however, modeling is required to create an effective feedforward controller, which takes advantage of the unique properties of IPMCs. The less accurate the model, the less reliable the feedforward controller becomes at predicting and manipulating the response of the system. A linear electromechanical model is used to describe the actuation behavior of an unsectored IPMC. The model is then expanded to include sectored IPMCs, using an assumption that the individual sectors are decoupled, that is, the motion of one sector doesn't appreciably affect that of another.

3.1 Previously Used IPMC Models

The complexity of the available models varies tremendously, from “black box” models (fitting a general form to empirical data) to “white box” models (developing a model based on physical operating principles of the system). Most models, however, fall somewhere in between. These “grey box” models begin with a physical basis for

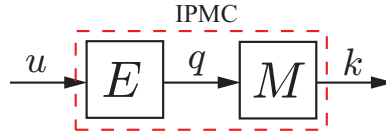


Figure 3.1: Electromechanical IPMC input-output model, where the input voltage u is mapped to charge q , and then the charge produces curvature k .

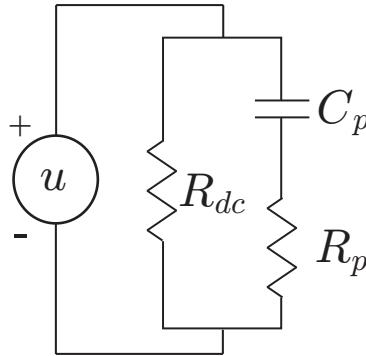


Figure 3.2: Clumped R-C model for IPMC electrical response [1, 46].

the model structure, and are further tuned to fit empirical data. In the modeling of IPMCs, it is convenient to separate the electrical and mechanical characteristics of the material. As depicted in Fig. 3.1, an electrical model (E) can be used to relate input voltage, $u(t)$, to the surface charge, $q(t)$, and then a separate electromechanical model (M) can relate the input charge to the mechanical output, curvature, $k(t)$. Many models have been created following this general structure, even if they are presented as a single, lumped model.

Linear resistive-capacitive (R-C) models are some of the simplest and most common models used to describe the electrical response of IPMCs. They can be “clumped,” where the entire actuator is modeled as a single circuit (see Fig. 3.2) [1, 46]. In this depiction, R_{dc} is the resistance drawing current at steady state, and R_p and C_p account for the capacitive nature of the actuator. One of the less accurate assumptions of this model is uniform voltage on the electrode surface. In actuality, there tends to be a significant voltage drop down the length of the IPMC, from the electrical

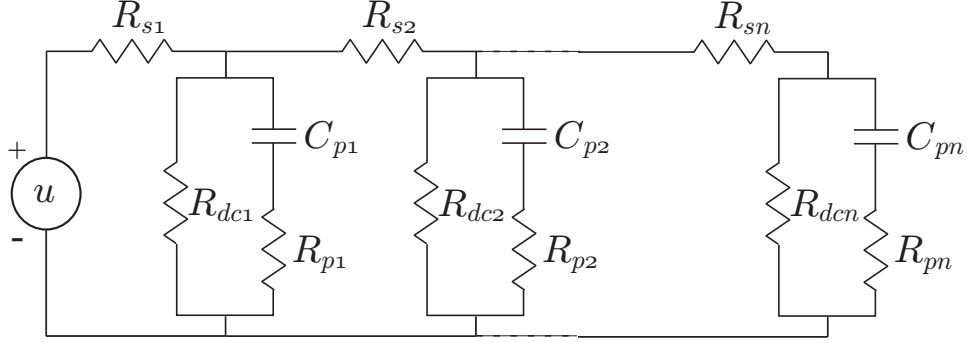


Figure 3.3: Distributed R-C model for IPMC electrical response [47–49].

contact to the free end. To account for this, the R-C model has been expanded to a “distributed” model (see Fig. 3.3), representing the IPMC as a series of R-C circuits, with a surface resistance, R_s , and voltage drop between each section [47–49].

As the electrical behavior of IPMCs is rather nonlinear, these linear models are limited to a relatively small voltage range, becoming increasingly less accurate with greater changes in voltage. More complicated nonlinear models have been developed in response to this. In [50], a nonlinear resistance was added to the clumped R-C model to account for the nonlinear behavior of the current absorbed by the IPMC. Another nonlinear circuit model was developed in [51]. This model is physics-based and only minimally reliant on empirical data. Nonlinear capacitance, ion diffusion resistance, pseudocapacitance due to electrochemical processes, and a nonlinear resistance of the polymer are explored. Finite element analysis (FEA) can be used to implement even more complex physics-based models without finding a closed form solution. In [52], for example, the IPMC charge dynamics are studied, implementing the Poisson-Nernst-Planck equations with FEA software.

Most IPMC electrical models have an associated electromechanical counterpart, relating the electrical response to the mechanical response. If the respective outputs and inputs are compatible, these models can be mixed and matched to suit the application. The electromechanical model paired with the R-C model in [46] is a simple

transfer function model with gain parameters weighting the effects of electrostatic and diffusion forces. Although it does not have a physical explanation, a model of the same form is used in [1]. In [47], the relationship between the electrical response and the resulting stress is modeled with a transfer function, and the motion is then evaluated with FEA methods. In [50], linear models are developed to relate the current (developed by a nonlinear model) to tip deflection and blocking force. The nonlinear electrical model in [51] is also followed up by a linear actuation model. Here, the charge density is related to stress in the IPMC, and ultimately the curvature of the actuator. In [52], charge density is related to the internal forces of the IPMC, and the motion is solved with FEA software. One alternative, monolithic description involves modeling the IPMC as a bimorph beam [9]. The material (considered homogenous) is assigned stiffness, piezoelectric, and permittivity matrices. The deformation can then be simulated using FEA methods, and a relatively low amount of computing power is needed.

Depending on the type of input signal, any of these models can be accurate and effective. Nonlinear models, however, can accurately predict the actuation behavior over a wider range of inputs. As the models become more physics-based, taking into account the physical mechanisms of actuation, the reliance on empirical data can be reduced and the models can become more universally applicable. In their current states, however, none of these approaches are perfect. More pertinent to this work is the fact that the more complex a model is, the less amenable it becomes to control development. Another important consideration is that many IPMC models do not account for back relaxation. The linear models presented here have a relaxation component, however, the more complex nonlinear models already presented do not. In [7], a nonlinear model is developed and implemented via FEA. To capture the back relaxation however, the simulation is broken up in a piecewise manner, with one set

of equations used for the forward motion for a brief time, followed by a different set of equations used to model the relaxation.

There has not been a great amount of work done with sectored IPMCs, and even less work has been done in the modeling effort. The model in [52] described earlier was used to describe the deformation of sectored IPMCs. In the FEA model, the sectors were electrically isolated, but beyond this there was not much consideration given to the unique nature of a sectored IPMC, which could be exploited in the control effort. Several multilink dynamic models have been developed for sectored IPMCs [4, 30, 53]. These models were designed to carefully illustrate the motion of each link, and the resulting complex bending. In this work, however, only simple bending is a concern, and given the sector configuration (described later), this kind of modeling is not necessary.

3.2 Conventional Unsectored IPMC Model

For simplicity, the R-C model developed in [46] is adapted here to describe the electrical response of the IPMC, as shown in Fig. 3.4. In this representation, $u(t)$ is the driving voltage and R_0 is the internal resistance of the voltage source. The R_1 - C branch accounts for the capacitive behavior of the IPMC, while R_2 accounts for the current that continues to flow even after an electrical steady state is reached. Using Thevenin equivalents to reduce the model down to a single resistor and capacitor, and applying Kirchhoff's voltage law (KVL) around the loop, the charge on the IPMC surface can be determined from the following equation:

$$R \frac{dq(t)}{dt} = \alpha u(t) - \frac{q(t)}{C}, \quad (3.1)$$

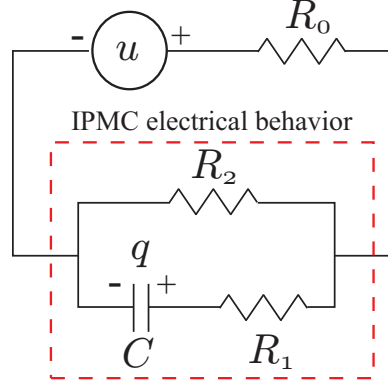


Figure 3.4: R-C model used to describe electrical response [46].

where

$$R = R_1 + \frac{R_0 R_2}{R_0 + R_2}, \quad (3.2)$$

and

$$\alpha = \frac{R_2}{R_0 + R_2}. \quad (3.3)$$

Converting to the Laplace domain and assuming zero initial conditions, the relationship between the input voltage $U(s)$ and surface charge $Q(s)$ can be given by the following transfer function:

$$\frac{Q(s)}{U(s)} = \frac{\alpha/R}{s + 1/\tau_1}, \quad (3.4)$$

where $\tau_1 = RC$ is the time constant of the circuit.

The electromechanical model is also adapted from [46], and is chosen because it is simple and accounts for back relaxation. In this model, the IPMC motion is governed by three factors: (1) the charge accumulated on the electrodes, (2) the rate of change of surface charge, and (3) the curvature. More specifically, if an IPMC is subjected to a step voltage, there is a quick initial forward motion which is dominated by the ionic flux through the IPMC. Mobile cations are drawn to the charging cathode, and carry water molecules across the membrane. This leads to swelling on the cathode

side of the IPMC and bending toward the anode. This ionic current is related to the surface charge rate, and as such, the forward motion fades as the electrodes become fully charged. At this point, back relaxation sets in, caused by the pressure gradient due to the water imbalance inside the IPMC. The water pressure lessens as the curvature decreases and the water molecules move closer to equilibrium. The back pressure is opposed by the lingering electrostatic force of the surface charge acting on the hydrated cations. When the electrostatic force balances the water pressure, motion ceases. This is one reason why the steady state position of the IPMC is rarely the same as the starting position. In this description, the motion of the actuator is modeled by

$$\frac{dk(t)}{dt} = K_1 \frac{dq(t)}{dt} - \frac{1}{\tau_2} [k(t) - K_2 q(t)], \quad (3.5)$$

where τ_2 is the time constant of the relaxation, and K_1 and K_2 are coefficients weighting the effects of the surface charge rate and of the surface charge, respectively. This single equation effectively describes the IPMC's actuation behavior, and needs only the surface charge and charge rate as inputs. Referring to the simple block diagram in Fig. 3.1, Eq. (3.5) represents the electromechanical model, M .

Converting Eq. (3.5) into the Laplace domain and assuming that the initial curvature is zero, that is $k(t = 0) = 0$, the linear charge solution Eq. (3.4) can be substituted for $Q(s)$ to produce the transfer function between curvature and input voltage:

$$\frac{K(s)}{U(s)} = \frac{K_{V1}}{\tau_1} \left[\frac{s + \frac{K_{V2}}{K_{V1}\tau_2}}{s^2 + \left(\frac{1}{\tau_1} + \frac{1}{\tau_2}\right)s + \frac{1}{\tau_1\tau_2}} \right], \quad (3.6)$$

where $K_{V1} = \alpha C K_1$ and $K_{V2} = \alpha C K_2$. For a step input of magnitude a , the time domain solution is

$$k(t) = a \left(K_{V2} - \frac{K_{V1}\tau_2 - K_{V2}\tau_1}{\tau_2 - \tau_1} e^{-\frac{t}{\tau_1}} + \frac{\tau_2(K_{V1} - K_{V2})}{\tau_2 - \tau_1} e^{-\frac{t}{\tau_2}} \right). \quad (3.7)$$

Nonlinear models such as the one given in [51] can be used; however a linear model may be more convenient for controller design and synthesis.

3.3 A Sectored IPMC Model

Next, the model described above is expanded to describe a sectored IPMC, that is an IPMC with patterned electrodes such as those described in [9]. Consider as an example an IPMC that has been partitioned into three electrically isolated regions as shown in Fig. 3.5(a). The electrodes are patterned such that the surface is symmetric about the longitudinal axis. For the IPMC shown, the outer portions are used as one sector (Sector 1) and are driven by input $u_1(t)$, while the middle portion is used as a second sector (Sector 2) and is driven by input $u_2(t)$. Thus, the IPMC consists of two controllable sectors. In this two-sector case, the IPMC is modeled as a dual input single output (DISO) system, in which the sectors of the IPMC are assumed to be decoupled and can be treated as independent systems. Although the curvature of the whole IPMC must physically be the same if simple bending is assumed, a “virtual” curvature can be obtained for each individual sector, defined as

$$K_i(s) = E_i(s)M_i(s)U_i(s), \quad (3.8)$$

where $K_i(s)$, $E_i(s)$, $M_i(s)$, and $U_i(s)$ are the curvature, electrical model, electromechanical model, and input voltage for the i^{th} sector, respectively. When each sector is activated, the sum of the virtual curvatures produces the net response of the complete IPMC, as is depicted in the model shown in Fig. 3.5(b). In this diagram, the final block for the i^{th} sector, $P_i(s)$, represents the conversion from curvature, $K_i(s)$, to tip displacement, $Y_i(s)$. Another transfer function could be used here, however in this study, the relationship is assumed to be linear, and the gain parameters in the elec-

tromechanical model of the i^{th} sector ($M_i(s)$) are tuned to produce tip displacements. From this point forward, the i^{th} sector will only be considered as a single transfer function model, $G_i(s)$, replacing $K_i(s)$ with $Y_i(s)$ in Eq. (3.6). For a general IPMC with n number of sectors, the total tip displacement is then given by

$$Y(s) = \sum_i^n U_i(s)G_i(s). \quad (3.9)$$

3.4 Summary

There are many approaches to the modeling of IPMCs from linear black box models to nonlinear, physics-based white box models. The latter could possibly be more accurate and more universal, although the application dictates what kind of model

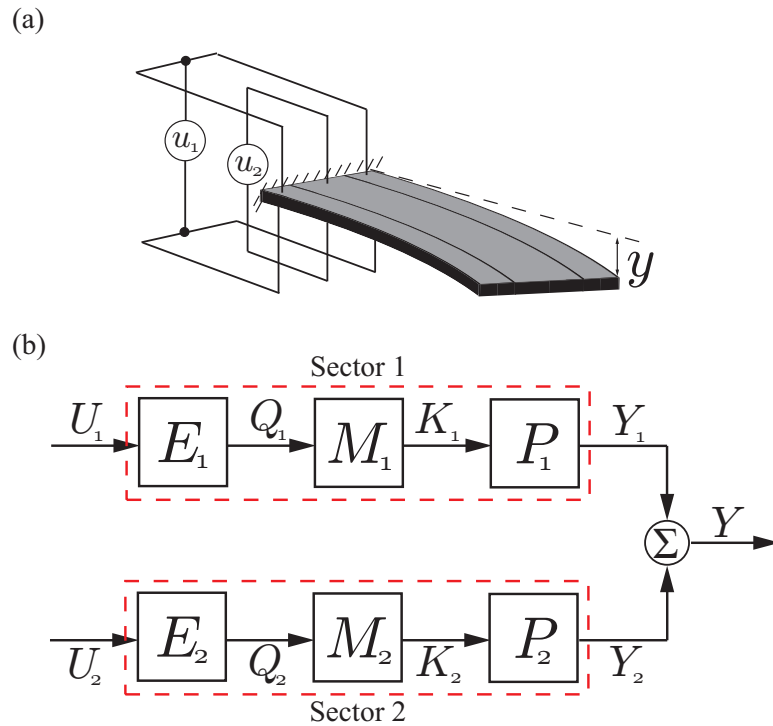


Figure 3.5: Sectored IPMC: (a) cantilever configuration with two inputs $u_1(t)$ (Sector 1) and $u_2(t)$ (Sector 2) and (b) the input-output model in the Laplace domain.

should be used. In this case, control is the end goal, so a balance between simplicity, versatility, and accuracy is key. Thus, basic linear models, with ties to the actual physical mechanisms acting on the IPMC, were used to describe the electrical and electromechanical behavior of the actuator. The model was expanded to predict the behavior of an IPMC with patterned electrodes, following the assumption that the sectors are decoupled, having a negligible effect on each other.

Chapter 4

Sector Control Strategy

In this chapter, the control approach is discussed. First, a feedforward technique is developed, utilizing the previously discussed concept of creating opposing back relaxation components on each sector. To have the relaxation components offset, the control input to one sector of the IPMC is set to the proper proportion via another controller and fed to the other sector. To aid in controller design, the actuation model is split into two components: one representing the forward motion of the IPMC and the other representing the back relaxation behavior. The previously discussed master-slave feedback technique is adapted to a feedforward architecture to suit this concept. Feedback is added to produce an integrated feedforward/feedback control scheme, more robust when faced with disturbances and other unmodeled effects. In this work, a simple proportional-integral (PI) feedback controller is designed, although many other options are available.

4.1 Feedforward Control Approach

To control the behavior of the sectored IPMC, the feedforward architecture in Fig. 4.1 is used. In this block diagram, $C_1(s)$ and $C_2(s)$ are the controllers associated with

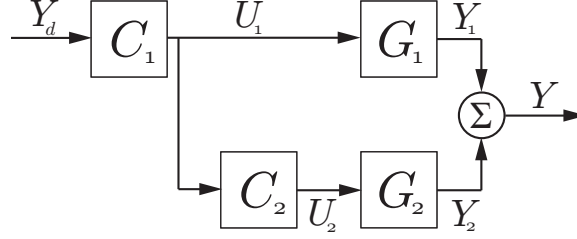


Figure 4.1: Feedforward control architecture for sectored IPMC.

Sector 1 and Sector 2, respectively, and $Y_d(s)$ is the desired trajectory. This structure is an open loop version of the master-slave control scheme given in [44]. This layout takes advantage of the assumption, described in Section 3.3, that the IPMC sectors are decoupled. As will be discussed further, the main objective of the feedforward stage is to cancel out the back relaxation components of each sector's motion. To achieve this, the input to Sector 2 will need to be dependent on Sector 1, so the levels of relaxation on each can be kept at the same magnitude. Master-slave structure allows for this kind of interaction. One advantage of the open-loop feedforward control approach is sensor feedback is not required; thus simplifying implementation. However, as described later, feedback control can be added to further improve performance, where feedback information can come from laser sensors, strain-based sensors [54], or other methods such as integrated PVDF films [49]. The specific layout of the master-slave structure can vary, but in this work, the input produced by $C_1(s)$ (the master controller) is fed into $C_2(s)$ (the slave controller). By inspection, the open-loop transfer function for this architecture is

$$T_{OL}(s) \triangleq \frac{Y(s)}{Y_d(s)} = C_1(s)[G_1(s) + C_2(s)G_2(s)]. \quad (4.1)$$

To aid in the design of the controllers, $C_1(s)$ and $C_2(s)$, the IPMC model for each sector, $G_i(s)$, is first broken into two separate transfer functions, one accounting for the quick forward movement of the IPMC ($G_{Fi}(s)$), and the other for the slow back

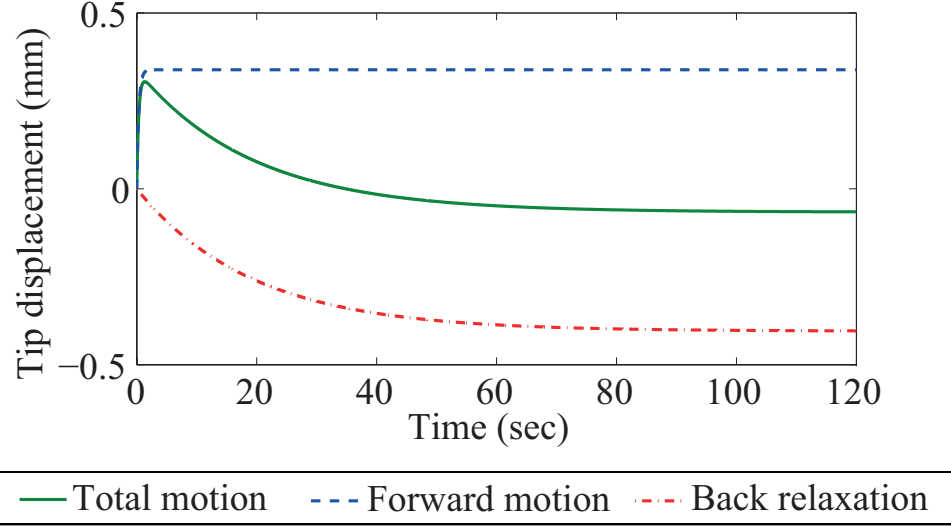


Figure 4.2: Simulated step responses of an IPMC's total motion, forward motion component, and back relaxation component.

relaxation ($G_{Bi}(s)$), composed of the constants (K_{V1i} , K_{V2i} , τ_{1i} , τ_{2i}) associated with the i^{th} sector. The transfer functions add to produce $G_i(s)$, as follows:

$$G_i(s) = G_{Fi}(s) + G_{Bi}(s) = \frac{A_i}{s + \frac{1}{\tau_{1i}}} + \frac{B_i}{s + \frac{1}{\tau_{2i}}}. \quad (4.2)$$

Equating coefficients, the following is obtained:

$$A_i = \frac{K_{V2i} - \frac{K_{V1i}\tau_{2i}}{\tau_{1i}}}{\tau_{1i} - \tau_{2i}} \quad (4.3)$$

and

$$B_i = \frac{K_{V1i}}{\tau_{1i}} + \frac{\frac{K_{V1i}\tau_{2i}}{\tau_{1i}} - K_{V2i}}{\tau_{1i} - \tau_{2i}}. \quad (4.4)$$

To illustrate this concept, Fig. 4.2 shows simulated step responses using a general $G_i(s)$ (total motion), $G_{Fi}(s)$ (forward motion component), and $G_{Bi}(s)$ (back relaxation component).

The slave controller, $C_2(s)$, is designed to counteract the back relaxation of Sec-

tor 1 by inducing back relaxation in the opposite direction for Sector 2. With the inputs properly weighted, the back relaxation effect of each sector roughly cancels. Then, $C_2(s)$ is responsible for setting $U_2(s)$ in proper proportion to $U_1(s)$, such that the sectors relax the same amount. Since $G_{Bi}(s)$ is responsible for the amount of relaxation in each sector, the following constraint must be satisfied for the relaxations to cancel,

$$U_1(s)G_{B1}(s) + U_2(s)G_{B2}(s) = 0, \quad (4.5)$$

and thus, $C_2(s)$ is given as

$$C_2(s) = \frac{U_2(s)}{U_1(s)} = -\frac{G_{B1}(s)}{G_{B2}(s)}. \quad (4.6)$$

Although $C_2(s)$ theoretically removes the back relaxation, the response is left offset, due to the opposing forward motions of the two sectors. To account for this, $U_1(s)$ must be gained by the master controller, $C_1(s)$, such that the forward motions add up to the desired level, dictated by $Y_d(s)$, that is

$$U_1(s)G_{F1}(s) + U_2(s)G_{F2}(s) = Y_d(s). \quad (4.7)$$

Rearranging and using Eq. (4.6) to substitute for $U_2(s)$, $C_1(s)$ becomes

$$C_1(s) = \frac{U_1(s)}{Y_d(s)} = \frac{1}{G_{F1}(s) + C_2(s)G_{F2}(s)}. \quad (4.8)$$

For $C_1(s)$, the numerator is of a higher degree than the denominator, making it an improper transfer function. To remedy this, a pole is added in the form of a low pass filter,

$$C_L(s) = \frac{a}{s + a}, \quad (4.9)$$

where a is the cutoff frequency, and is chosen to be much greater than the other poles of $C_1(s)$, to minimize the effect on the low frequency response. Without this filter in place, the open loop transfer function is equal to unity, meaning the feedforward controller would ideally provide a perfect response below the cutoff frequency of the filter, if the model used is perfect.

A key condition of stability for the feedforward approach is that the induced forward motion of Sector 2 can't completely counteract that of Sector 1. If this were allowed to happen, the magnitude of the voltage input to Sector 1 (and consequently, to Sector 2) would have to be constantly increased, while never achieving the desired position. For example, if the desired trajectory is positive, the following must be true for stability:

$$U_1(s)G_{F1}(s) + U_2(s)G_{F2}(s) > 0. \quad (4.10)$$

Rearranging Eq. 4.10, we find that the condition for stability is

$$G_{F1}(s) > -C_2(s)G_{F2}(s). \quad (4.11)$$

The only way to ensure that this condition is met is to properly tailor the IPMC sectors so they fit this relationship. The proper methods to design the sectors, however, are beyond the scope of this work.

4.2 Adding Feedback Control

To account for disturbances, nonlinearity, and other undesirable factors not captured in the model, a feedback controller ($C_0(s)$) is integrated with the feedforward controller. As shown in Fig. 4.3, the feedback loop is set up such that the feedforward and feedback inputs ($U_{ff}(s)$ and $U_{fb}(s)$, respectively) are added to yield $U_1(s)$. Although this is not typical for a master-slave controller, this structure is chosen so the

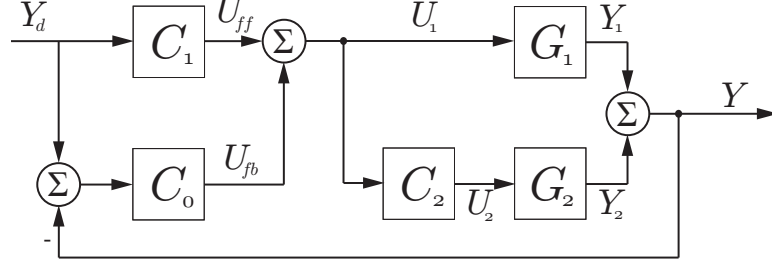


Figure 4.3: Block diagram of integrated feedforward/feedback control scheme.

feedforward controller is still active even if the feedback controller is disabled. This can be seen in the closed-loop transfer function for the feedforward/feedback system:

$$T_{CL}(s) \triangleq \frac{Y(s)}{Y_d(s)} = \frac{C_0(s)[G_1(s) + C_2(s)G_2(s)]}{1 + C_0(s)[G_1(s) + C_2(s)G_2(s)]} + \frac{C_1(s)[G_1(s) + C_2(s)G_2(s)]}{1 + C_0(s)[G_1(s) + C_2(s)G_2(s)]}. \quad (4.12)$$

If $C_0(s)$ is set equal to zero, Eq. (4.1) and Eq. (4.12) are identical. The feedback controller $C_0(s)$ can be chosen as desired provided it yields a stable closed-loop system. Given the structure shown in Fig. 4.3, the feedback controller can be considered to be in series with a single plant, $G_1(s) + C_2(s)G_2(s)$, and can be designed to improve the response of this system.

In this work, however, it is important to compare the integrated feedforward/feedback strategy with simple feedback control. To give a fair comparison, the feedback controller is designed to control the IPMC as if it was unsectored, without the additional controller, $C_2(s)$. A model is developed, $G_{tot}(s)$, for the response of the IPMC with the sectors actuated in unison and used to design a simple proportional-integral (PI) feedback controller,

$$C_0(s) = K_p + \frac{K_{int}}{s}, \quad (4.13)$$

where K_p and K_{int} are proportional and integral gains, respectively. The controller

is designed to achieve zero steady state error with less than 5% overshoot. The overshoot (OS) is used to determine the desired damping ratio (ζ) of the closed loop system, as follows:

$$\zeta = \frac{|\ln(OS)|}{\sqrt{|\ln(OS)|^2 + \pi^2}}. \quad (4.14)$$

The desired natural frequency (ω_n) and proportional gain (K_p) are then determined by equating coefficients of the desired characteristic polynomial for the closed loop system under proportional control:

$$s^2 + \left(\frac{1}{\tau_1} + \frac{1}{\tau_2}\right)s + \frac{1}{\tau_1\tau_2} + K_p = s^2 + 2\zeta\omega_n s + \omega_n^2. \quad (4.15)$$

To limit the effect on the transient response, the integral gain (K_{int}) is typically chosen to be much lower than the proportional gain. As the focus of this work is the tracking of low-frequency signals, the integral gain could be chosen to be relatively high. The ratio of K_{int} to K_p in this work ranged from five to ten times greater than $\zeta\omega_n$. Both gains produced using this method can be rather high, so to reduce excessive sensitivity to disturbances, the gains are scaled down while maintaining their relative proportions.

4.3 Summary

A feedforward approach was taken to cancel out back relaxation by applying properly weighted opposing voltage signals to the two sectors of the IPMC. Feedback control was integrated as well, using a simple PI controller to increase the robustness of the system to disturbances and other effects not captured in the model. PI control was used for the sake of simplicity, however there are surely even more effective options.

Chapter 5

The Experimental System

All the concepts and methods developed thus far must be experimentally tested to prove their validity, and the details of implementation are discussed in this chapter. It is important to develop a sound experimental setup to ensure that the results are accurate and reliable. First, the fabrication process is given, including procedures to plate the Nafion[®] membrane and then to pattern the electrodes. The test setup is then described, outlining the key pieces of equipment used to conduct the experiments. Finally, the model is experimentally validated, and the process for fitting the gain parameters within the model is described.

5.1 IPMC Fabrication and Electrode Patterning

For this study, all IPMCs are fabricated in-house, using a platinum reduction method similar to that described by Kim and Shahinpoor [14]. The ion exchange membrane used is Nafion[®] (1100 EW) with a thickness of 0.5 mm. This thickness is chosen because it displays a good balance between speed and force in actuation. To increase surface area for the reduction process, the membrane is roughened with sandpaper. All sanding is done in the transverse direction, to promote greater bending. After

soaking the membrane in deionized (DI) water for several hours, it is cleaned in successive baths of hydrogen peroxide (H_2O_2) and sulfuric acid (H_2SO_4), followed by two baths in DI water. The plating process begins by introducing platinum ions to the membrane by soaking it in a platinum complex solution, tetraamineplatinum chloride hydrate ($\text{Pt}[\text{NH}_3]_4\text{Cl}_2$), overnight. Metallic platinum is formed on the surface via a reducing agent, sodium borohydride (NaBH_4). Ammonium hydroxide (NH_4OH) is also added during the reduction process to regulate the pH of the solution. After the reduction, the plated membrane is washed in sulfuric acid and two DI water baths. The plating process is repeated until a desirable surface resistance is reached. The plated IPMCs are cut down to sheets with dimensions of approximately $50 \text{ mm} \times 10 \text{ mm}$. Finally, the platinum electrodes are patterned as necessary, using a sharp blade. The outer electrode portions are each roughly 3 mm across, and the middle section is approximately 4 mm across. After a great amount of testing, the surface resistance of the IPMCs degrade. When this happens, the IPMCs are revitalized by adding a layer of gold over the platinum layer. While immersed in a gold solution, a low voltage is applied between the IPMC and a piece of stainless steel, leading to electroplating of gold onto the IPMC [12].

5.2 IPMC Test Setup

A custom-designed voltage/current amplifier is used to drive the IPMCs in this study [54]. To provide a strong clamping force and resist corrosion, nickel plated neodymium magnets are used to conduct power to the IPMCs [12,27]. A mount for the magnets is designed to hold the magnets in place, so each would only contact one sector of the IPMC surface electrode (see Fig. 5.1). In this case, the IPMC is divided into three sections, meaning six magnets are used. The outer two sections are actuated in unison, however, making them effectively one sector. MATLAB, in con-

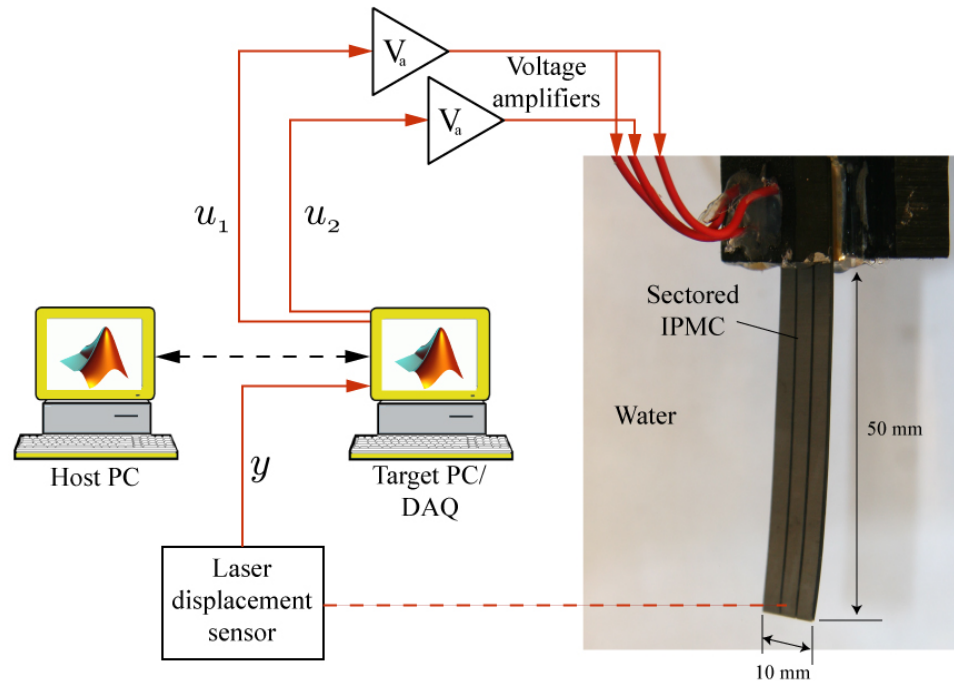


Figure 5.1: Experimental setup for underwater actuation, including an IPMC with two effective sectors.

junction with Simulink and xPC target, is used to run the experiments. In Simulink, the various control architectures can easily be constructed in a block diagram format, as shown in Fig. 5.2. Then, using xPC target, the Simulink model is loaded from a host computer to a target computer, which is setup to run only the simulation, and no other background programs. The target computer communicates with a 12-bit data acquisition card, which serves to output the voltage signals, as well as record the IPMC tip displacement, via a laser displacement sensor (SUNX Microlaser Sensor LM10, with a resolution of $1 \mu\text{m}$ and a bandwidth of 10 Hz). An additional amplifier and filter is used to improve the signal-to-noise ratio of the laser output signal. All tests were conducted underwater, in a small tank.

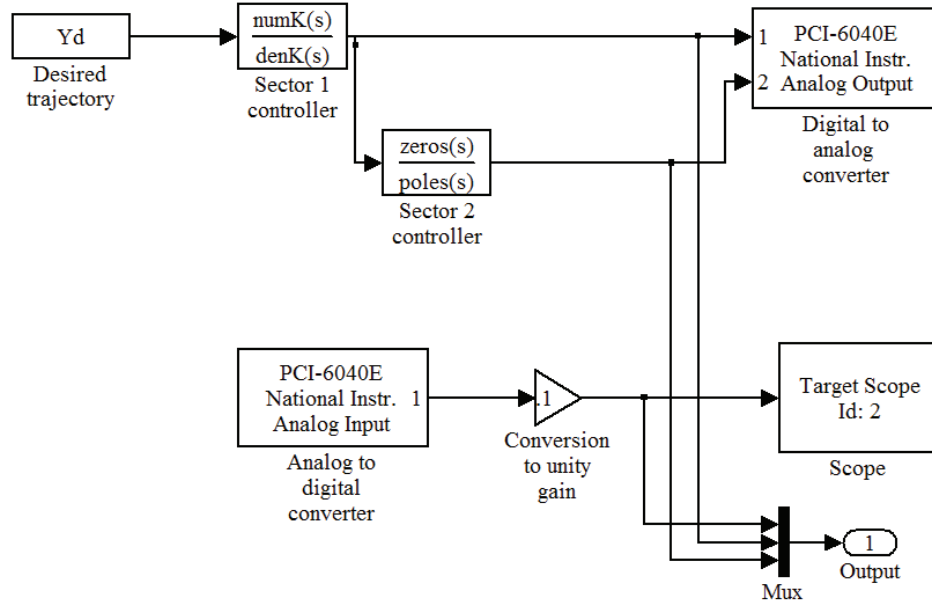


Figure 5.2: Simulink block diagram for feedforward tests.

Table 5.1: Gain parameters for model validation.

Sector	K_{V1}	K_{V2}	τ_1	τ_2
1	0.430	0.146	0.531	35.543
2	0.243	0.115	0.652	19.224

5.3 Model Validation

A key assumption in modeling the sectored IPMC is that the sectors are decoupled. To validate this assumption, the sectors of an IPMC are actuated individually with a step input of 1 V [see Fig.5.3(a)]. Then, the same step input is given to both sectors at the same time and the tip displacement is compared to the sum of the tip displacements for the individual actuation tests, as shown in Fig. 5.3(b). The results are in good agreement, providing confidence in the decoupled assumption.

To determine the various gain parameters for the previously described model, each sector of the IPMC is subjected to a step input, and the displacement is recorded. A step input is used for the model fitting process because it excites all of the dynamics of

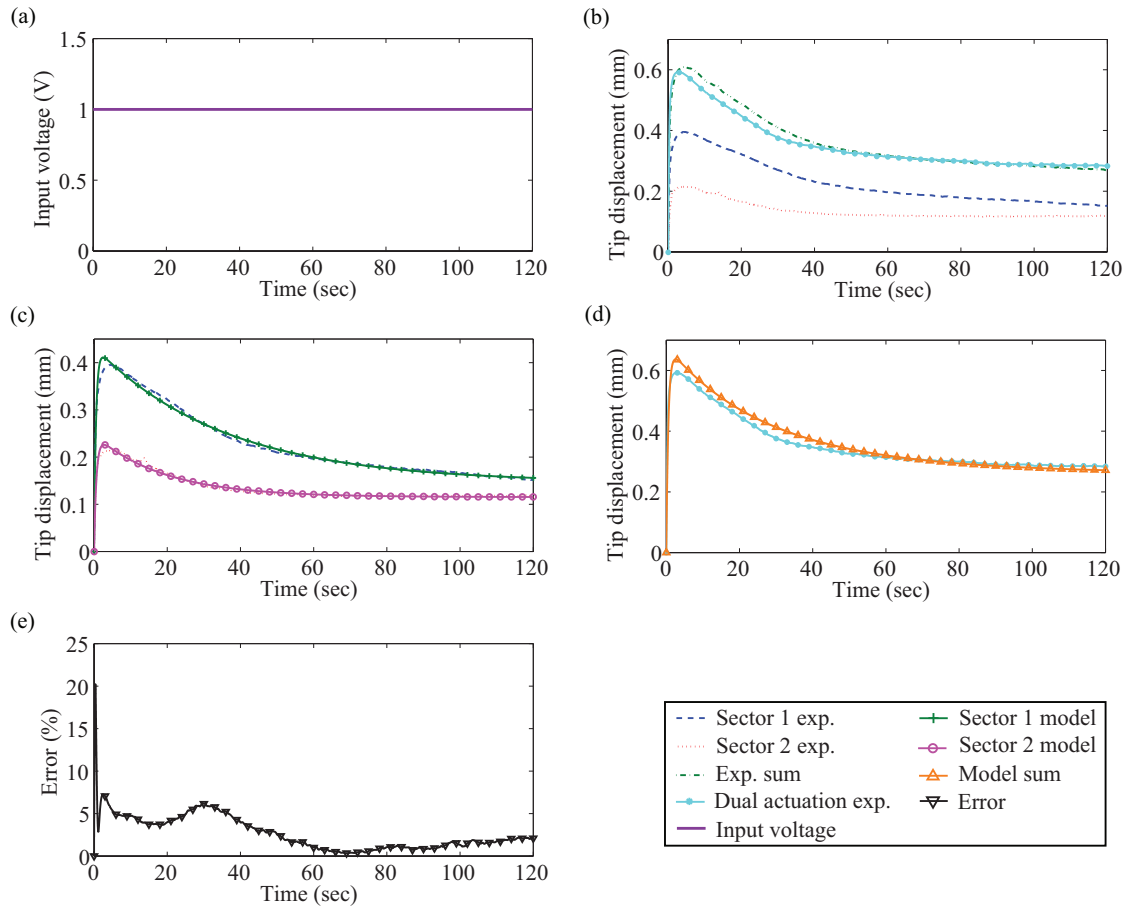


Figure 5.3: Model validation: (a) input voltage for all tests, (b) individual and simultaneous sector actuation, (c) individual sector responses and corresponding simulation results, (d) simultaneous sector actuation and sum of corresponding simulations, and (e) error between simultaneous sector actuation and sum of corresponding simulations.

the IPMC. Using a least squares curve fit in MATLAB, the model, $G_i(s)$, is tuned to fit the data for each sector. The gain parameters had to be adjusted periodically as the response of the IPMC changed, however the gain parameters used for this model validation experiment are given in Table 5.1. The model is then implemented in Simulink to carry out all simulations, as well as the experiments in conjunction with the xPC target system. Figure 5.3(c) compares experimental sectored IPMC step responses and the corresponding simulations. Finally, the decoupled assumption is further verified by comparing the sum of the model responses to the experimental IPMC response when both sectors are actuated simultaneously. As shown in Fig. 5.3(d), the model represents the true response reasonably well. The corresponding error, defined as

$$e(t) = \left[\frac{|y(t) - y_d(t)|}{\max[y_d(t)] - \min[y_d(t)]} \right] \times 100\%, \quad (5.1)$$

is given in Fig. 5.3(e), and is found to be less than 10% for the majority of the test. The Root-Mean-Square (RMS) error over the total testing time, T , is defined as

$$e_{RMS} = \left[\frac{\sqrt{\frac{1}{T} \int_0^T [y(t) - y_d(t)]^2 dt}}{\max[y_d(t)] - \min[y_d(t)]} \right] \times 100\%, \quad (5.2)$$

and is found to be 3.73%, providing good confidence in the modeling process.

5.4 Summary

The experimental system was described, including the fabrication of the actuators and the equipment used for testing. Experiments were also conducted to validate the model, and illustrate the process for tuning the model to fit measured responses.

Chapter 6

Experimental Results

In this chapter, the results yielded from implementing the control techniques developed in Chapter 4 are shown. For several waveforms, the response is shown for open loop, feedforward, and feedforward/feedback cases. The latter two techniques are found to significantly reduce the error compared to the open loop case. The results of a test using pure feedback control are also given for reference. The control techniques developed here are shown to reduce the input voltage substantially, as compared to the pure feedback case. As a final indication of the power of these methods, an IPMC is shown holding a steady deflection for a period of twenty minutes under bounded input voltages and with no back relaxation.

6.1 Open Loop Response

Although step inputs were used to identify the model parameters, an alternative signal is chosen for these experiments. It is desirable to have a smooth reference trajectory, to avoid large spikes in the control inputs. An exponential function of the form $y_d(t) = D(1 - \exp(-\tau t))$ is used as a reference trajectory, where D is the steady state value of the function, and τ is the time constant. In these tests, D was chosen

to be relatively small (0.4 mm) to keep the input voltages low and within the more linear range of operation of the IPMC. Furthermore, for these tests, $\tau = 2$.

First an open loop response is taken as a control, supplying the input

$$u(t) = \frac{1}{y_{max}} y_d(t), \quad (6.1)$$

to both sectors, where y_{max} is the modeled maximum value of a simultaneous step response for both sectors. To determine y_{max} , Eq. (3.6) is fit to an experimental simultaneous step response for both sectors, producing the single model, G_{tot} , for the whole IPMC. Using the resulting gain parameters, the derivative of Eq. (3.7) is taken. Setting the derivative equal to zero, the time of the maximum displacement, t_{max} , is found. This time is then plugged back into Eq. (3.7) to find the maximum value, y_{max} . The open loop response and corresponding tracking error are given in Fig. 6.1(a) and (b), respectively.

6.2 Feedforward Control Response

Next, the feedforward control alone is implemented for the same reference trajectory, significantly improving the response [see Figs. 6.1(a) and (b)], as compared to the open loop case. The maximum error, found by taking the maximum of Eq. (5.1) and Root-Mean-Square (RMS) error, calculated with Eq. (5.2), are given in Table 6.1. In this case, the RMS error is improved by approximately 85%. Furthermore, the input voltages supplied to the IPMC [see Fig. 6.1(c)] are bounded, implying that the position of the IPMC can be maintained for extended periods of time.

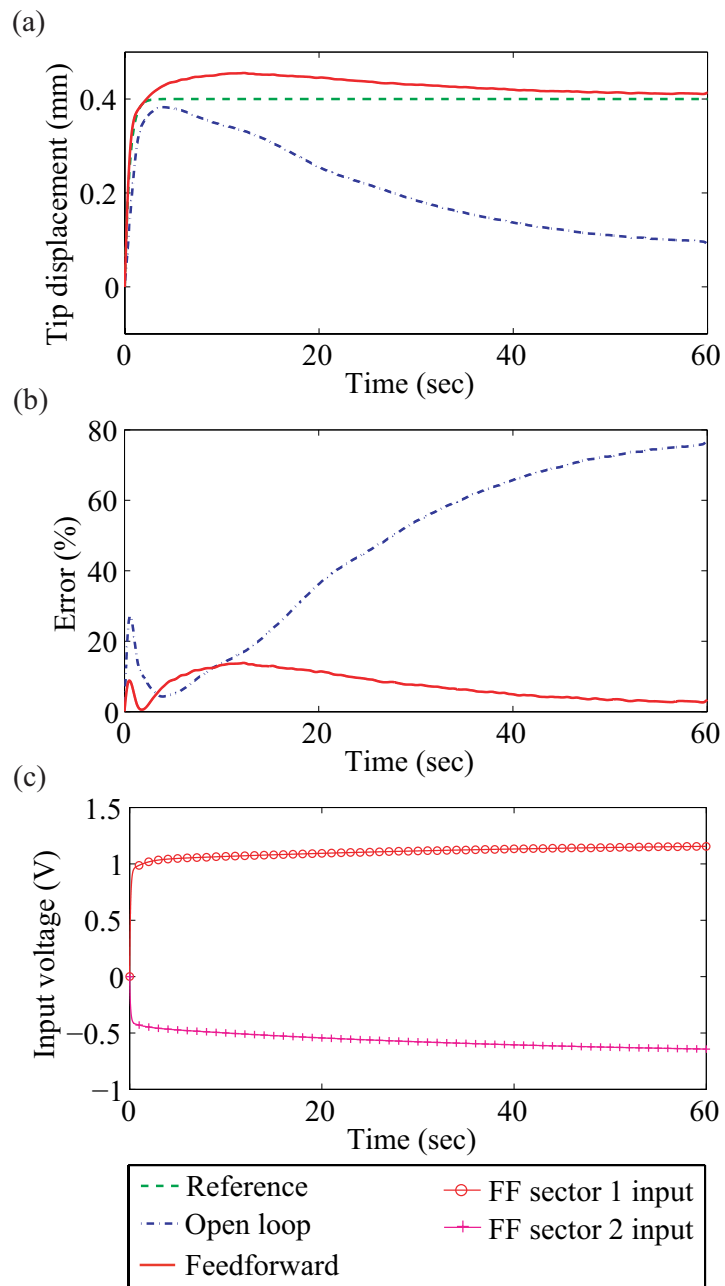


Figure 6.1: Open loop and feedforward responses to exponential reference: (a) tip displacement, (b) tracking error, and (c) feedforward input voltages.

6.3 Feedforward/Feedback Control Response

The integrated feedforward/feedback controller is then implemented to further reduce the error. The feedback gains are developed as previously described, and then scaled down to much lower values to ensure that the feedback controller is not dominant. The gains are varied as the model is refit, but for this example, $K_p = 0.5$ and $K_{int} = 3.41$. The response is again improved [see Figs. 6.2(a) and (b)]. In this case, the RMS tracking error is improved by nearly 97%, as compared to the open loop case. All tracking errors are given in Table 6.1.

To illustrate the improvement this technique offers over traditional feedback control, a longer test is conducted, comparing the integrated feedforward/feedback control case to a simple feedback control case. In the latter case, the previously developed feedback controller is used without the feedforward controller, treating the sectored IPMC as a non-sectored IPMC. The tip displacement and input voltage (identical for each sector in the simple feedback case) are given in Figs. 6.3(a) and (b), respectively. It is observed that simple feedback produces an increasing input voltage as expected to maintain a constant position in the presence of back relaxation. A voltage threshold is imposed to prevent damage to the IMPC, and once it is reached, the IPMC quickly relaxes. For this sort of feedback to be effective, the voltage must be able to rise freely, but this can lead to serious damage of the actuator, as previously discussed.

Another advantage of the integrated feedforward/feedback control method over traditional feedback is a significantly reduced power consumption. To demonstrate this reduction, the previously described voltage threshold was removed, allowing the feedback controller to freely raise the control input voltage as needed to maintain the tip position [see Fig. 6.4(a)]. As shown in Fig. 6.4(b), the power consumption in the pure feedback case ramps up over time and becomes much greater than the

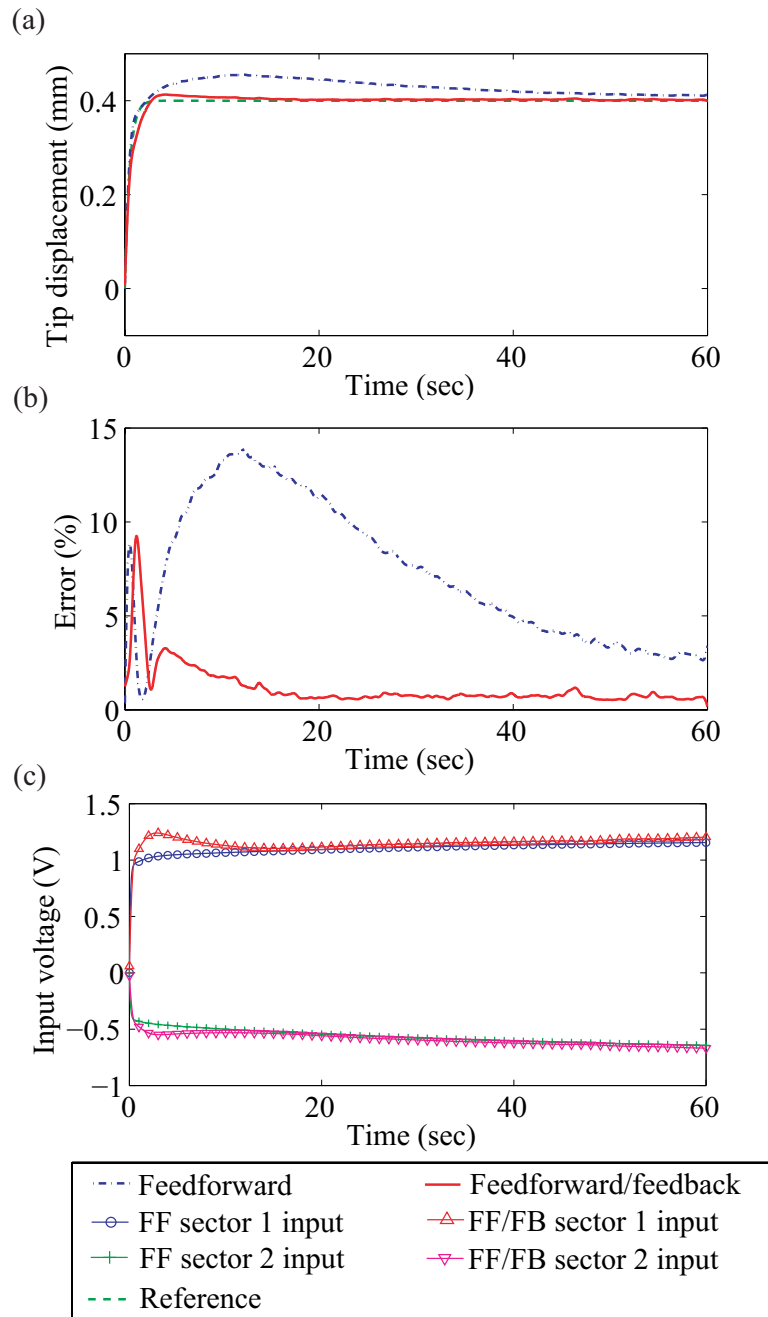


Figure 6.2: Feedforward and feedforward/feedback responses to exponential reference: (a) tip displacement, (b) tracking error, and (c) input voltages.

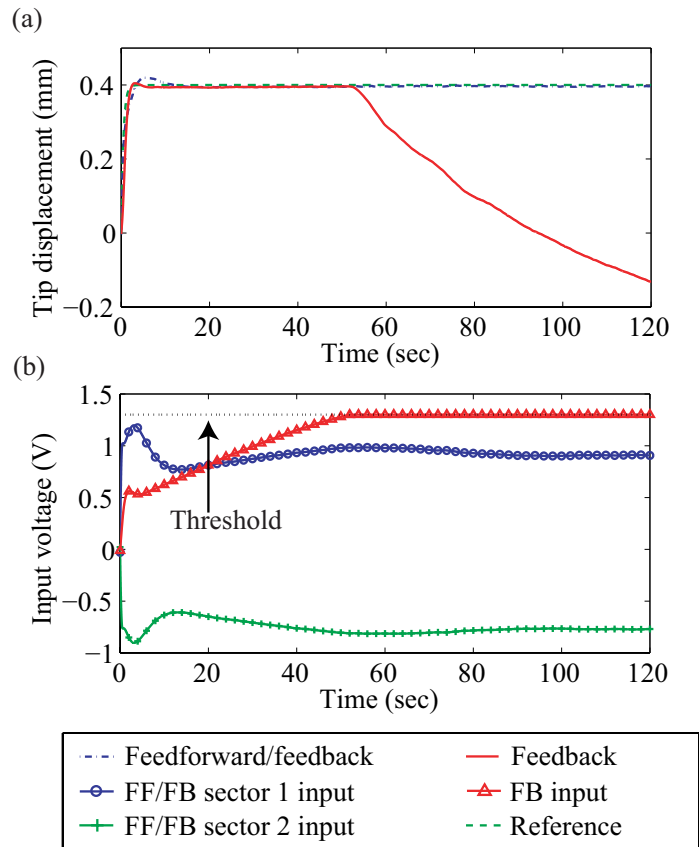


Figure 6.3: Feedback response to exponential reference with input voltage threshold: (a) tip displacement and (b) input voltages.

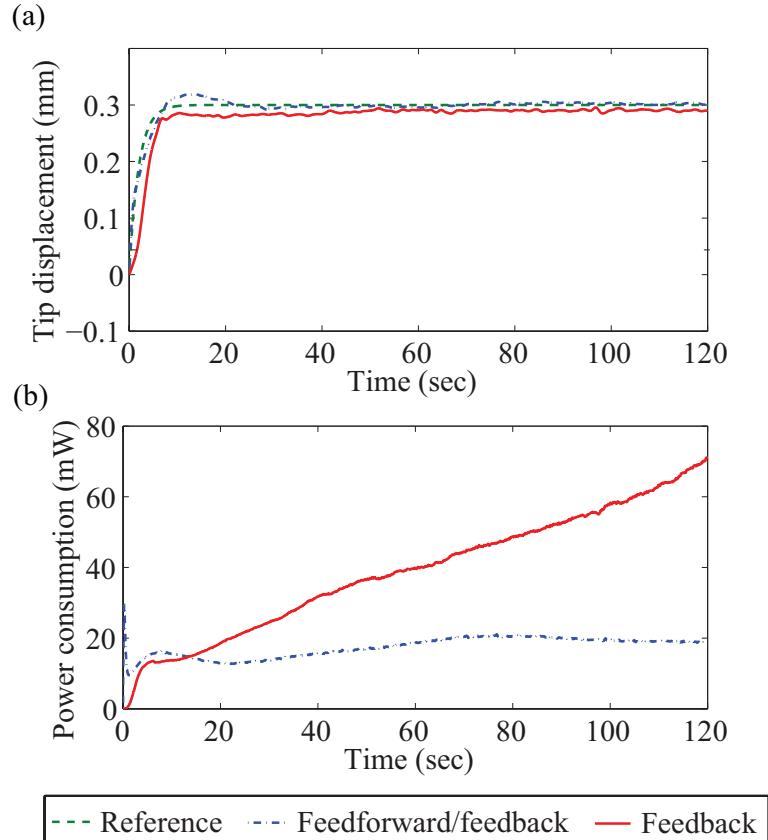


Figure 6.4: Feedback response to exponential reference without input voltage threshold: (a) tip displacement and (b) power consumption.

power consumption for the integrated feedforward/feedback case. In these tests, the RMS error is lower for the feedforward/feedback case (3.94%, compared to 6.88% for pure feedback). Without the voltage threshold, there is a greater risk of damage to the IPMC, so the steady state value and time constant of the reference signal were changed to $D = 0.3$ mm and $\tau = 0.5$, respectively, to reduce the feedback control input.

Table 6.1: Feedforward/feedback control results.

	Open loop	Feedforward	Improvement over open loop	Feedforward /feedback	Improvement over open loop
e_{max} (%)	77.20	13.85	82.06	9.25	88.02
e_{RMS} (%)	53.03	8.13	84.67	1.71	96.78

6.4 Alternative Waveforms

To further verify the effectiveness of this method, more complex waveforms are also used as reference trajectories. The IPMC's response under open loop, feedforward, feedback, and feedforward/feedback control to sinusoidal, triangular, and trapezoidal waveforms with a non-zero DC component are given in Figs. 6.5, 6.6, and 6.7 respectively. In these tests, it is noted that although the feedback control input is not always greater than the other control inputs, it does appear to increase at a greater rate. Finally, the IPMC is subjected to the previously described exponential reference under feedforward/feedback control for a period of twenty minutes (1200 seconds). With the proposed control technique, the IPMC is able to maintain a steady position for the entire period with bounded inputs to both sectors, as shown in Fig. 6.8. It should be noted that under open loop conditions, the IPMC in this study begins to relax after approximately 10 seconds. In this control test, there was no sign of relaxation for a period 120 times longer.

6.5 Summary

This chapter presented the results of experiments using the developed feedforward and feedforward/feedback control techniques. Tracking error was significantly improved compared to the open loop case, and input voltages were reduced compared to the pure feedback case.

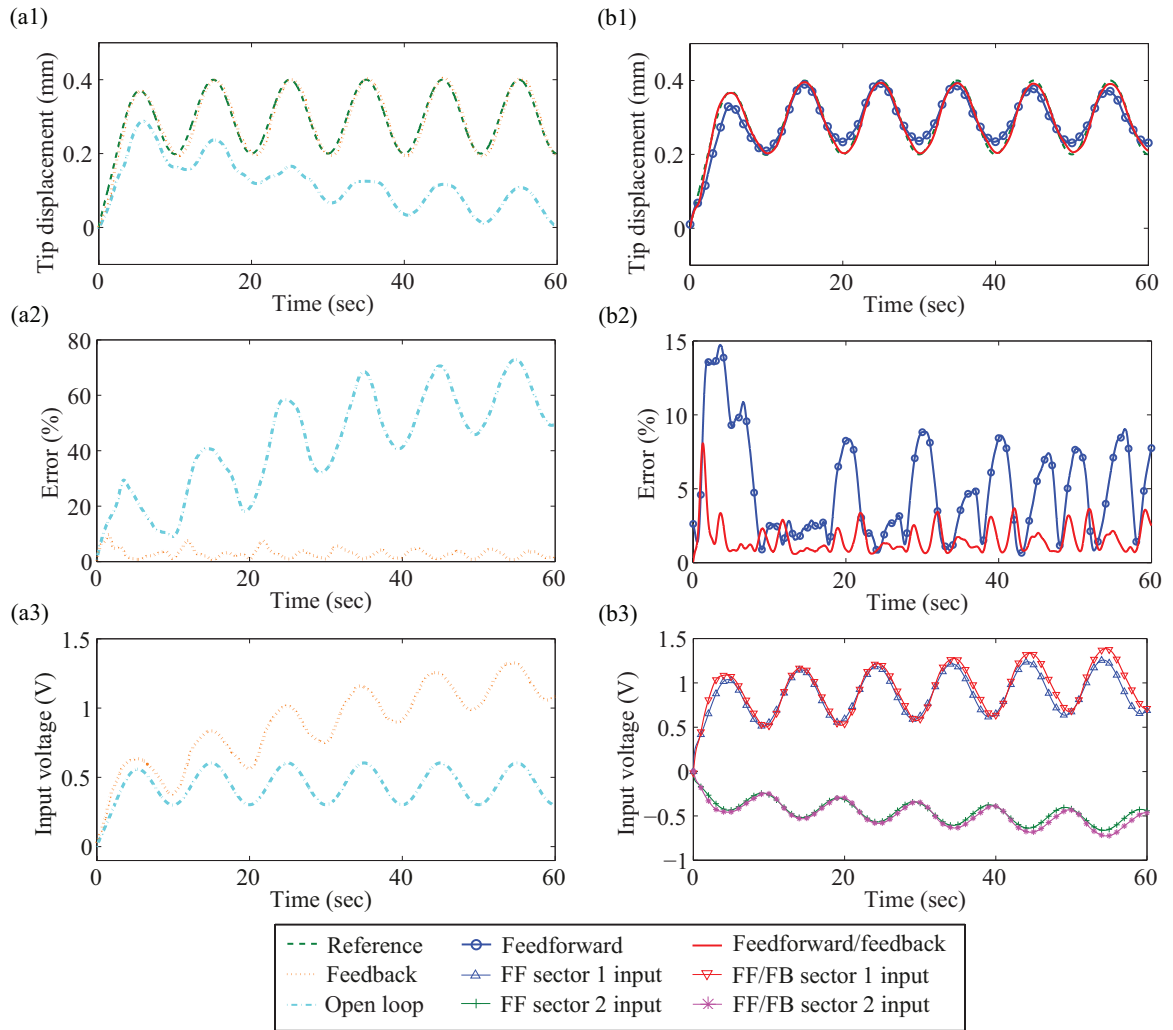


Figure 6.5: Sectored IPMC with a sinusoidal reference: (a) open loop and pure feedback control, and (b) feedforward and feedforward/feedback control.

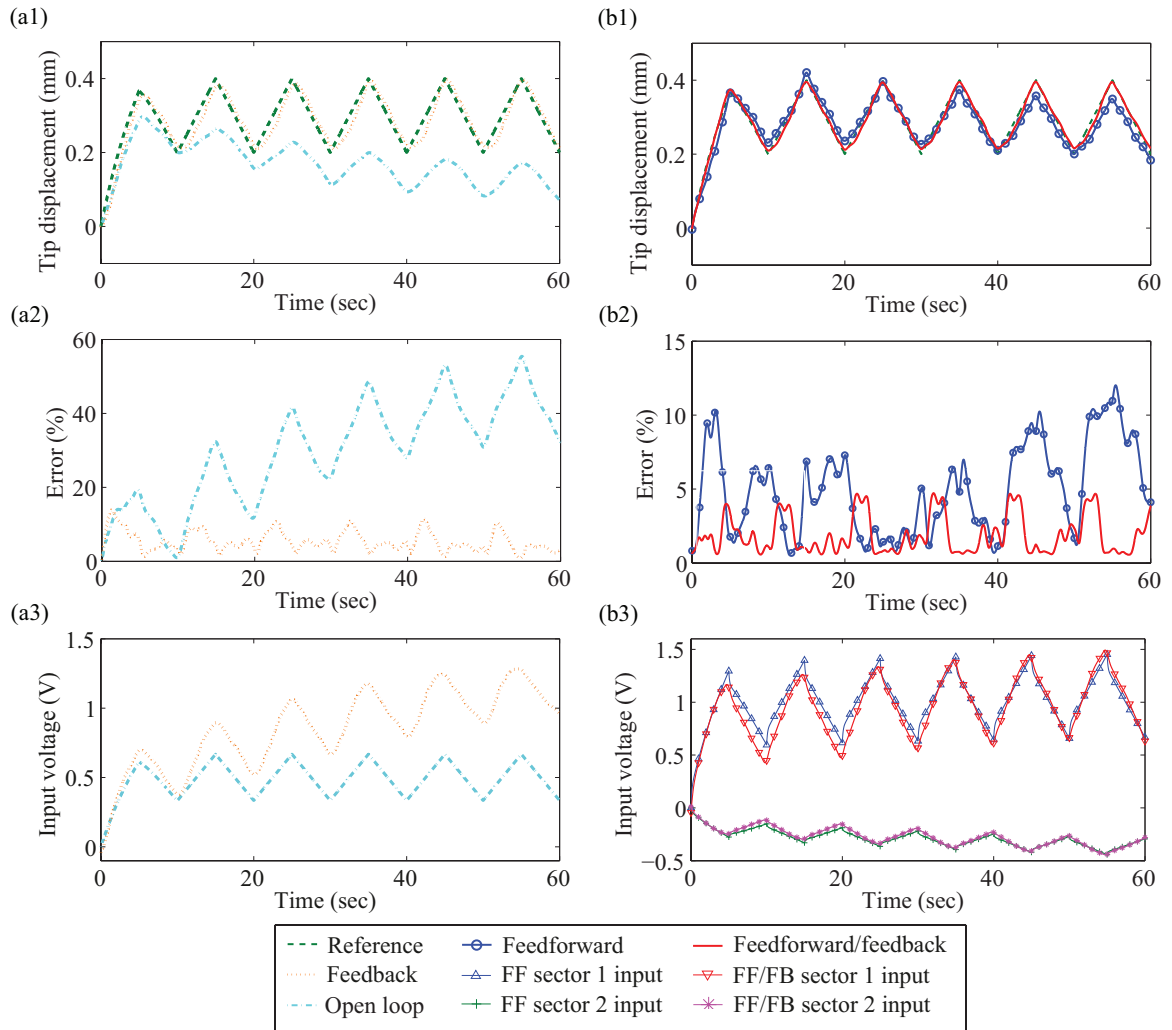


Figure 6.6: Sectored IPMC with a triangular reference: (a) open loop and pure feedback control, and (b) feedforward and feedforward/feedback control.

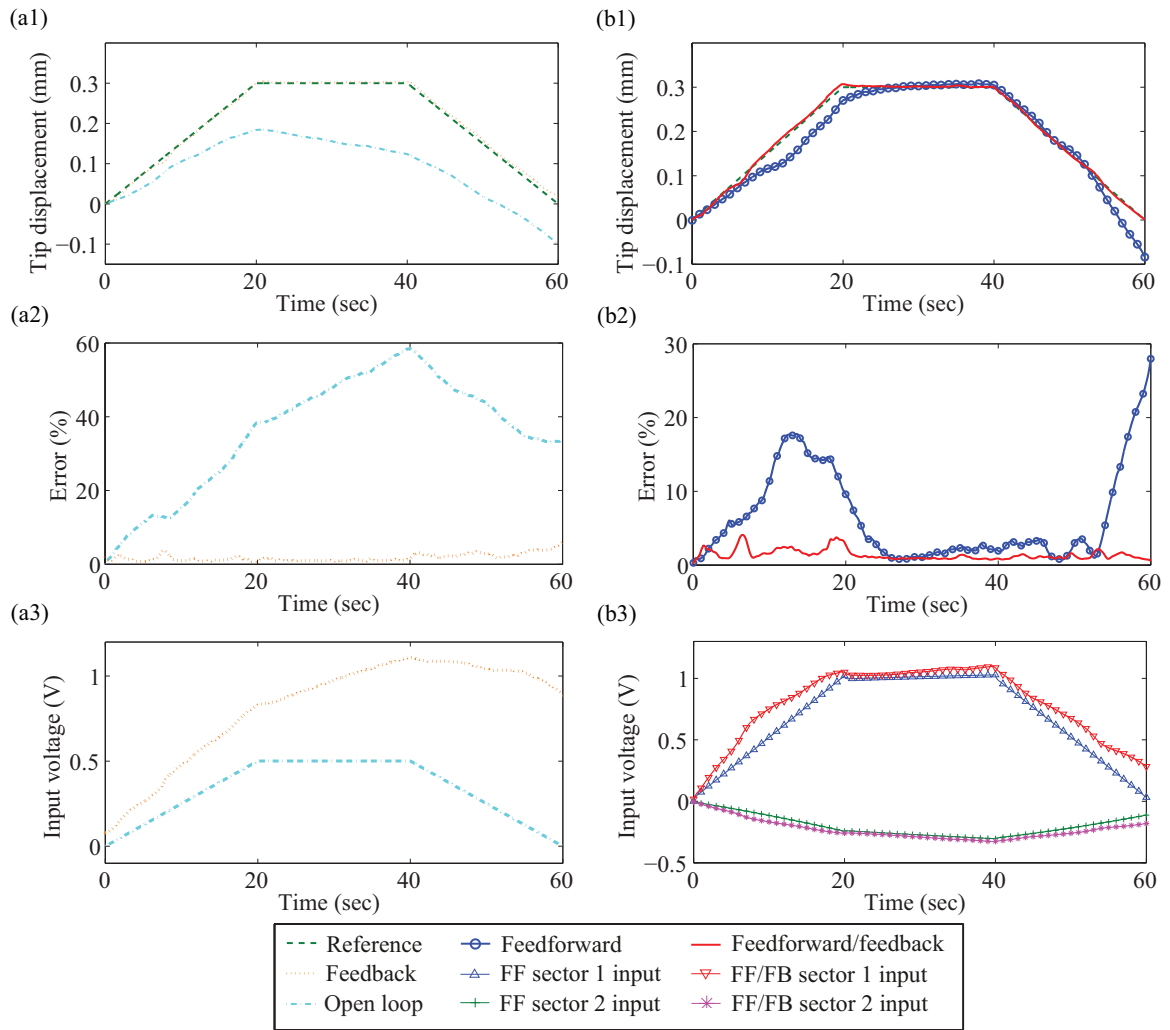


Figure 6.7: Sectored IPMC with a trapezoidal reference: (a) open loop and pure feedback control, and (b) feedforward and feedforward/feedback control.

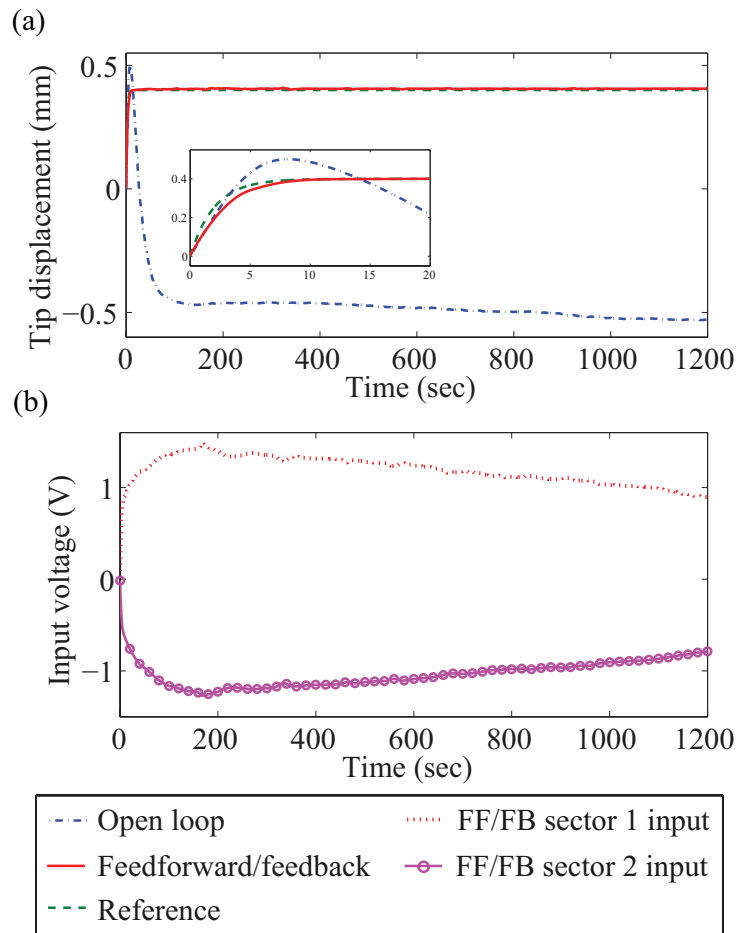


Figure 6.8: Sectored IPMC with a twenty-minute exponential reference: (a) response and (b) input.

Chapter 7

Conclusions

This paper explored controlled activation of patterned electrodes on IPMCs to mitigate back relaxation. It was found that a decoupled actuation model can reasonably be applied to a sectored IPMC, when used for simple bending. Using this assumption, a technique was developed to fight back relaxation, using an IPMC with two sectors, and driving the sectors in opposite directions. When properly weighted, the opposing relaxation components can offset each other, while still achieving the desired forward motion. A feedforward controller was developed, based on this principle, and was found to significantly improve the response of an IPMC subjected to references with large DC components, which would normally induce considerable back relaxation. For a steady reference, where the IPMC is meant to have constant tip deflection, the feedforward control approach yielded an approximately 85% improvement in the tracking error as compared to the open loop case. To further improve the tracking performance of the system, a feedback controller was added. The integrated feedforward/feedback approach is intended to make the system more robust when faced with nonlinearities, disturbances, and other factors not captured in the model. The error was further reduced with this approach, yielding nearly a 97% improvement in tracking error as compared to the open loop case.

One key advantage of this method is the minimal additional fabrication that must be performed. Starting with a typical IPMC, the only additional work necessary to enable this style of control is to pattern the electrodes, which can be done after the plating process is complete. The other main advantage is the reduced control inputs supplied to the IPMC, as compared to the pure feedback control case. The control inputs have been shown to be bounded within reasonable values for an extended period of time.

Of course, the methods described in this work are not perfect. The range of use of this method is heavily dependent on the accuracy of the model. As described, a linear model was used in this work. While this simplified the control design process, it limited the operating range of the IPMC, because of the nonlinear behavior experienced by the actuator. This work is also hindered by the available knowledge of the relationship between electrode patterning and IPMC performance. The IPMCs were sectored following general concepts of motion, however, little is known about the nuances of the effect patterning can have on the amounts of forward motion and back relaxation.

Chapter 8

Future Work

The primary limitation of this work is that the model used is linear, and cannot perfectly capture the behavior of an IPMC over a large voltage range. Although thorough nonlinear models have been created, as was discussed in Chapter 3, they can be relatively complex and more difficult to use in the control process than their linear counterparts. However, for progress to be made, future work should include the use of a more accurate nonlinear model. The better the model can represent the true response of the IPMC, the more effective the feedforward controller can be. Ideally, the feedforward controller would be robust enough to be used independently, without integrated feedback. Although it is unlikely that the sectored IPMC could be effectively used in a practical application (especially underwater robotics) without some kind of feedback, any improvement in the feedforward performance can somewhat reduce the dependence on the feedback element. This could mean less accurate and less expensive equipment could be used for feedback. For instance, if the sensor feedback was not as integral, using an expensive laser displacement sensor or an inexpensive strain gage could potentially yield performances of equal quality.

Also vital to the progression of this work is a better understanding of the sectoring process and the effect it has on the performance of an IPMC. In this work, the sectors

were only designed with the criteria of symmetry, and making Sector 1 larger than Sector 2, under the assumption it would produce a stronger response. Beyond this however, there is much to learn about how the sectors should be designed. The design likely affects the stability under feedforward control, and there are surely alternative designs capable of yielding better performance.

Bibliography

- [1] K. J. Kim, W. Yim, J. W. Paquette, and D. Kim, "Ionic polymer-metal composites for underwater operation," Journal of Intelligent Material Systems and Structures, vol. 18, no. 2, pp. 123–131, 2007.
- [2] N. Kamamichi, M. Yamakita, K. Asaka, and L. Zhi-Wei, "A snake-like swimming robot using IPMC actuator/sensor," in IEEE International Conference on Robotics and Automation, 2006, pp. 1812–1817.
- [3] M. Aureli, V. Kopman, and M. Porfiri, "Free-locomotion of underwater vehicles actuated by ionic polymer metal composites," IEEE/ASME Transactions on Mechatronics, vol. 15, no. 4, pp. 603–614, 2010.
- [4] W. Yim, J. Lee, and K. J. Kim, "An artificial muscle actuator for biomimetic underwater propulsors," Bioinspiration & Biomimetics, vol. 2, no. 2, pp. S31–S41, 2007.
- [5] M. J. Lee, S. H. Jung, S. Lee, M. S. Mun, and I. Moon, "Control of IPMC-based artificial muscle for myoelectric hand prosthesis," in The First IEEE/RAS-EMBS International Conference on Biomedical Robotics and Biomechatronics, 2006, pp. 1172–1177.
- [6] M. Shahinpoor and K. J. Kim, "Ionic polymer-metal composites: IV. industrial and medical applications," Smart Materials and Structures, vol. 14, no. 1, p. 197, 2005.
- [7] W. J. Yoon, P. G. Reinhall, and E. J. Seibel, "Analysis of electro-active polymer bending: A component in a low cost ultrathin scanning endoscope," Sensors and Actuators A: Physical, vol. 133, no. 2, pp. 506–517, 2007.
- [8] J. H. Jeon, S. W. Yeom, and I. K. Oh, "Fabrication and actuation of ionic polymer metal composites patterned by combining electroplating with electroless plating," Composites Part A: Applied Science and Manufacturing, vol. 39, no. 4, pp. 588–596, 2008.
- [9] K. J. Kim, D. Pugal, and K. K. Leang, "A twistable ionic polymer-metal composite artificial muscle for marine applications," Marine Technology Society Journal, vol. 45, no. 4, pp. 83–98, 2011.

- [10] Y. Shan and K. K. Leang, "Frequency-weighted feedforward control for dynamic compensation in ionic polymer-metal composite actuators," Smart Materials and Structures, vol. 18, no. 12, p. 125016, 2009.
- [11] S. Nemat-Nasser, "Micromechanics of actuation of ionic polymer-metal composites," Journal of Applied Physics, vol. 92, no. 5, pp. 2899–2915, 2002.
- [12] J. Hubbard, M. Fleming, K. K. Leang, V. Palmre, D. Pugal, and K. J. Kim, "Characterization of sectored-electrode IPMC-based propulsors for underwater locomotion," in ASME Conference on Smart Materials, Adaptive Structures and Intelligent Systems (SMASIS), Scottsdale, AZ, 2011, pp. 171–180.
- [13] B. Fang, C. Lin, and M. Ju, "Development of sensing/actuating ionic polymer-metal composite (IPMC) for active guide-wire system," Sensors and Actuators A: Physical, vol. 158, no. 1, pp. 1–9, 2009.
- [14] K. J. Kim and M. Shahinpoor, "Ionic polymer-metal composites: II. manufacturing techniques," Smart Materials and Structures, vol. 12, no. 1, pp. 65–80, 2003.
- [15] D. Bandopadhyaya, "Quasi-static tip positioning of multi-segmented IPMC for micro-manipulation following Euler-Bernoulli and pseudo-rigid body model," Journal of Reinforced Plastics and Composites, vol. 28, no. 6, pp. 743–764, 2009.
- [16] Z. Chen, X. Tan, and M. Shahinpoor, "Quasi-static positioning of ionic polymer-metal composite (IPMC) actuators," in Proceedings of the 2005 IEEE/ASME International Conference on Advanced Intelligent Mechatronics, 2005, pp. 60–65.
- [17] J. W. Paquette, K. J. Kim, J. D. Nam, and Y. S. Tak, "An equivalent circuit model for ionic polymer-metal composites and their performance improvement by a clay-based polymer nano-composite technique," Journal of Intelligent Material Systems and Structures, vol. 14, no. 10, pp. 633–642, 2003.
- [18] S. M. Kim and K. J. Kim, "Palladium buffer-layered high performance ionic polymer-metal composites," Smart Materials and Structures, vol. 17, no. 3, p. 035011, 2008.
- [19] G. H. Feng, "Numerical study on dynamic characteristics of micromachined ionic polymer metal composite devices based on molecular-scale modeling," Computational Materials Science, vol. 50, no. 1, pp. 158–166, 2010.
- [20] E. Shoji and D. Hirayama, "Effects of humidity on the performance of ionic polymer-metal composite actuators: Experimental study of the back-relaxation of actuators," The Journal of Physical Chemistry B, vol. 111, no. 41, pp. 11 915–11 920, 2007.

- [21] S. Nemat-Nasser and Y. Wu, “Comparative experimental study of ionic polymer-metal composites with different backbone ionomers and in various cation forms,” Journal of Applied Physics, vol. 93, no. 9, p. 5255, 2003.
- [22] B. Kim, D. Kim, J. Jung, and J. Park, “A biomimetic undulatory tadpole robot using ionic polymer-metal composite actuators,” Smart Materials and Structures, vol. 14, no. 6, pp. 1579–1585, 2005.
- [23] S. Guo, L. Shi, X. Ye, and L. Li, “A new jellyfish type of underwater microrobot,” in International Conference on Mechatronics and Automation, 2007, pp. 509–514.
- [24] S. Yeom and I. Oh, “A biomimetic jellyfish robot based on ionic polymer metal composite actuators,” Smart Materials and Structures, vol. 18, no. 8, p. 085002, 2009.
- [25] Z. Chen, T. I. Um, and H. Bart-Smith, “A novel fabrication of ionic polymer-metal composite membrane actuator capable of 3-dimensional kinematic motions,” Sensors and Actuators A: Physical, vol. 168, no. 1, pp. 131–139, 2011.
- [26] S. Guo, Y. Ge, L. Li, and S. Liu, “Underwater swimming micro robot using IPMC actuator,” in Proceedings of the 2006 IEEE International Conference on Mechatronics and Automation, 2006, pp. 249–254.
- [27] S. McGovern, G. Alici, V. T. Truong, and G. Spinks, “Finding NEMO (novel electromaterial muscle oscillator): a polypyrrole powered robotic fish with real-time wireless speed and directional control,” Smart Materials and Structures, vol. 18, no. 9, p. 095009, 2009.
- [28] Z. Chen and X. Tan, “Monolithic fabrication of ionic polymer-metal composite actuators capable of complex deformation,” Sensors and Actuators A: Physical, vol. 157, no. 2, pp. 246–257, 2010.
- [29] G. Feng and R. Chen, “Fabrication and characterization of arbitrary shaped μ IPMC transducers for accurately controlled biomedical applications,” Sensors and Actuators A: Physical, vol. 143, no. 1, pp. 34–40, 2008.
- [30] Y. Nakabo, T. Mukai, and K. Asaka, “Kinematic modeling and visual sensing of multi-DOF robot manipulator with patterned artificial muscle,” in Proceedings of the 2005 IEEE International Conference on Robotics and Automation (ICRA), Barcelona, Spain, 2005, pp. 4315–4320.
- [31] K. Kruusamae, P. Brunetto, S. Graziani, A. Punning, G. Di Pasquale, and A. Aabloo, “Self-sensing ionic polymer-metal composite actuating device with patterned surface electrodes,” Polymer International, vol. 59, no. 3, pp. 300–304, 2009.

- [32] H. Nakadoi, D. Sobey, M. Yamakita, and T. Mukai, "Liquid environment-adaptive IPMC fish-like robot using extremum seeking feedback," in IEEE/RSJ International Conference on Intelligent Robots and Systems (IROS), 2008, pp. 3089–3094.
- [33] Y. Shan, "Fabrication and integrated feedforward and feedback control of ionic polymer-metal composite actuators," Master's thesis, Virginia Commonwealth University, 2008.
- [34] M. Shahinpoor, Y. Bar-Cohen, J. O. Simpson, and J. Smith, "Ionic polymer-metal composites (IPMCs) as biomimetic sensors, actuators and artificial muscles - a review," Smart Materials and Structures, vol. 7, no. 6, p. R15, 1998.
- [35] B. Kim, S. Park, C. Y. Jee, and S. Yoon, "An earthworm-like locomotive mechanism for capsule endoscopes," in IEEE/RSJ International Conference on Intelligent Robots and Systems, 2005, pp. 2997–3002.
- [36] S. Nemat-Nasser, S. Zamani, and Y. Tor, "Effect of solvents on the chemical and physical properties of ionic polymer-metal composites," Journal of Applied Physics, vol. 99, no. 10, pp. 104902–17, 2006.
- [37] Y. Bar-Cohen, S. Leary, A. Yavrouian, K. Oguro, S. Tadokoro, J. Harrison, J. Smith, and J. Su, "Challenges to the application of IPMC as actuators of planetary mechanisms," in Proceedings of the SPIE Smart Structures and Materials Symposium, vol. 3987, Newport, CA, 2000, pp. 140–146.
- [38] J. Lee and Y. Yoo, "The structure and performance of ionic polymer-metal composite actuators prepared via electroless plating process using various alcohols," Macromolecular Symposia, Special Issue: Advanced Polymer for Emerging Technologies, vol. 249-250, no. 1, pp. 56–60, 2007.
- [39] D. Kim and K. J. Kim, "Experimental investigation on electrochemical properties of ionic polymer-metal composite," Journal of Intelligent Material Systems and Structures, vol. 17, no. 5, pp. 449–454, 2006.
- [40] N. D. Bhat and W. J. Kim, "Precision force and position control of ionic polymer-metal composite," Journal of Systems and Control Engineering, vol. 218, no. 6, pp. 421–432, 2004.
- [41] K. Mallavarapu and D. J. Leo, "Feedback control of the bending response of ionic polymer actuators," Journal of Intelligent Material Systems and Structures, vol. 12, no. 3, pp. 143–155, 2001.
- [42] S. Kang, J. Shin, S. J. Kim, H. J. Kim, and Y. H. Kim, "Robust control of ionic polymer-metal composites," Smart Materials and Structures, vol. 16, no. 6, pp. 2457–2463, 2007.

- [43] B. Fang, M. Ju, and C. Lin, "A new approach to develop ionic polymer-metal composites (IPMC) actuator: Fabrication and control for active catheter systems," Sensors and Actuators A: Physical, vol. 137, no. 2, pp. 321–329, 2007.
- [44] S. J. Schroeck, W. C. Messner, and R. J. McNab, "On compensator design for linear time-invariant dual-input single-output systems," IEEE/ASME Transactions on Mechatronics, vol. 6, no. 1, pp. 50–57, 2001.
- [45] A. A. Mamun, I. Mareels, T. H. Lee, and A. Tay, "Dual stage actuator control in hard disk drive - a review," in The 29th Annual Conference of the IEEE Industrial Electronics Society, 2003, vol. 3, 2003, pp. 2132–2137.
- [46] X. Bao, Y. Bar-Cohen, and S. S. Lih, "Measurements and macro models of ionomeric polymer-metal composites (IMPC)," in Proceedings of the SPIE Smart Structures and Materials Symposium, EAPAD Conference, vol. 4695, San Diego, CA, 2002, pp. 220–227.
- [47] R. Kanno, S. Tadokoro, T. Takamori, M. Hattori, and K. Oguro, "Linear approximate dynamic model of ICPF (ionic conducting polymer gel film) actuator," in Proceedings of the 1996 IEEE International Conference on Robotics and Automation (ICRA), vol. 1, 1996, pp. 219–225.
- [48] M. Shahinpoor and K. J. Kim, "The effect of surface-electrode resistance on the performance of ionic polymer-metal composite (IPMC) artificial muscles," Smart Materials and Structures, vol. 9, no. 4, pp. 543–551, 2000.
- [49] Z. Chen, Y. Shen, N. Xi, and X. Tan, "Integrated sensing for ionic polymer-metal composite actuators using PVDF thin films," Smart Materials and Structures, vol. 16, no. 2, pp. S262–S271, 2007.
- [50] C. Bonomo, L. Fortuna, P. Giannone, S. Graziani, and S. Strazzeri, "A nonlinear model for ionic polymer metal composites as actuators," Smart Materials and Structures, vol. 16, no. 1, p. 1, 2007.
- [51] Z. Chen, D. R. Hedgepeth, and X. Tan, "A nonlinear, control-oriented model for ionic polymer-metal composite actuators," Smart Materials and Structures, vol. 18, no. 5, p. 055008, 2009.
- [52] D. Pugal, K. Kim, and A. Aabloo, "An explicit physics-based model of ionic polymer-metal composite actuators," Journal of Applied Physics, vol. 110, no. 8, p. 084904, 2011.
- [53] P. Arena, C. Bonomo, L. Fortuna, M. Frasca, and S. Graziani, "Design and control of an IPMC wormlike robot," IEEE Transactions on Systems, Man, and Cybernetics, Part B: Cybernetics, vol. 36, no. 5, pp. 1044–1052, 2006.

- [54] K. K. Leang, Y. Shan, S. Song, and K. J. Kim, “Integrated sensing for IPMC actuators using strain gages for underwater applications,” IEEE/ASME Transactions on Mechatronics, vol. 17, no. 2, pp. 345–355, 2012.